The Canadian Mineralogist
Vol. 42, pp. 515-537 (2004)

ZONED SULFIDES AND SULFARSENIDES OF THE PLATINUM-GROUP ELEMENTS FROM THE PENIKAT LAYERED COMPLEX, FINLAND

ANDREI Y. BARKOV[§] AND MICHAEL E. FLEET[§]

Department of Earth Sciences, University of Western Ontario, London, Ontario N6A 5B7, Canada

ROBERT F. MARTIN[§]

Department of Earth and Planetary Sciences, McGill University, 3450 University Street, Montreal, Quebec H3A 2A7, Canada

TUOMO T. ALAPIETI[§]

Department of Geology, Institute of Geosciences, University of Oulu, FIN–90401 Oulu, Finland

ABSTRACT

Compositional zoning and some unusual microtextures are observed in sulfides and sulfarsenides of the platinum-group elements (PGE) [laurite – erlichmanite, irarsite – hollingworthite, and vysotskite – braggite series] from the Kirakkajuppura PGE deposit in the Penikat layered complex, Finland. This unique deposit locally contains exceptionally high concentrations of the PGE in altered sulfur-poor mafic–ultramafic rocks, resulting in numerous unusual species of platinum-group minerals (PGM). Various mechanisms of charge-balance substitution are formulated to explain incorporation of Ir, Rh, and Fe in laurite – erlichmanite, and of Ru and Fe in irarsite – hollingworthite. Complexly zoned grains of laurite – erlichmanite and irarsite – hollingworthite crystallized from a liquid as primary phases in a closed system. The fine-scale zoning observed in the laurite – erlichmanite reflects rapid fluctuations in $f(S_2)$, whereas a decrease in temperature during crystallization may have been crucial in controlling the behavior and distribution of minor amounts of Fe. Late zones of vysotskite, which are relatively rich in Pd and Ni, are developed in Pt-rich members of the vysotskite – braggite series and display an intimate association with abundant micro-aggregates and bands of a hydrous silicate(s). These zones formed by a hydrothermal alteration of the original vysotskite – braggite. Thus, Pd, Ni, Pt, and the associated lithophile elements were mobile in a late-stage fluid during the alteration.

Keywords: platinum-group elements, platinum-group minerals, sulfides, sulfarsenides, laurite, erlichmanite, irarsite, hollingworthite, vysotskite, braggite, zoning, substitution schemes, Kirakkajuppura deposit, Penikat layered complex, Finland.

SOMMAIRE

Nous décrivons la zonation et certaines microtextures inhabituelles dans les sulfures et sulfarséniures des éléments du groupe du platine (EGP) [séries laurite – erlichmanite, irarsite – hollingworthite, et vysotskite – braggite] provenant du gisement à EGP de Kirakkajuppura, faisant partie du complexe stratiforme de Penikat, en Finlande. Ce gisement unique contient des concentrations anormalement élevées en EGP dans des roches mafiques et ultramafiques relativement dépourvues en soufre, ce qui a provoqué la cristallisation de plusieurs espèces rares de minéraux du groupe du platine. Nous précisons plusieurs mécanismes de substitution et d'équilibrage des charges pour expliquer l'incorporation de l'Ir, du Rh, et du Fe dans la laurite – erlichmanite, et du Ru et du Fe dans l'irarsite – hollingworthite. Des grains de laurite – erlichmanite et d'irarsite – hollingworthite fortement zonés ont cristallisé à partir d'un liquide comme phases primaires dans un système fermé. La zonation fine de la laurite – erlichmanite témoigne de fluctuations rapides en $f(S_2)$, tandis qu'une diminution en température au cours de la cristallisation pourrait avoir été critique pour régir le comportement et la distribution des quantités mineures de Fe. Des zones tardives de vysotskite, qui sont relativement riches en Pd et Ni, sont développées dans les membres riches en Pt de la série vysotskite – braggite et montrent une association intime avec une abondance de micro-aggrégats et d'accumulations de silicate(s) hydraté(s). Ces zones se sont formées par altération hydrothermale d'un membre de la série vysotskite – braggite. C'est donc dire que Pd, Ni, Pt, et les éléments lithophiles associés étaient mobiles dans une phase fluide tardive lors de l'altération.

(Traduit par la Rédaction)

Mots-clés: éléments du groupe du platine, minéraux du groupe du platine, sulfures, sulfarséniures, laurite, erlichmanite, irarsite, hollingworthite, vysotskite, braggite, zonation, schémas de substitution, gisement de Kirakkajuppura, complexe stratiforme de Penikat, Finlande.

§ *E-mail addresses*: abarkov@uwo.ca, mfleet@uwo.ca, bobm@eps.mcgill.ca, tuomo.alapieti@oulu.fi

Introduction

The Kirakkajuppura platinum-group element (PGE) deposit within the Sompujärvi PGE reef forms part of the Early Proterozoic Penikat layered complex in the Fennoscandian Shield (Alapieti & Lahtinen 1986, 1989, Halkoaho *et al.* 1990, Alapieti & Halkoaho 1995). This deposit is extraordinary among PGE deposits hosted by various layered complexes worldwide. Locally, unusually high concentrations, exceeding 0.5 kg/t total PGE, are observed in altered mafic–ultramafic rocks at Kirakkajuppura. These rocks are very poor in S (typically less than 200 ppm S), and are nearly free of base-metal sulfides (BMS). The platinum-group mineralogy of the Kirakkajuppura deposit is of particular interest because of the presence of some unique or very uncommon platinum-group minerals (PGM), such as unnamed Pd–Pb oxide (Barkov *et al.* 1999a), various Fe–Cu–PGE thiospinels (Barkov *et al.* 2000), laflammeite ($Pd_3Pb_2S_2$: Barkov *et al.* 2002) and a likely unnamed (Fe-dominant) analogue of konderite (Barkov *et al.* 2004a).

In this paper, we continue our characterization of various PGM and their associations observed in the Kirakkajuppura PGE deposit, and present representative results of a total of eight hundred original wavelength-dispersion electron-microprobe analyses. Our main purposes here are: (1) to describe various patterns of zoning and characteristic textures observed in the PGE sulfides [laurite (RuS_2) – erlichmanite (OsS_2), and vysotskite (PdS) – braggite (Pt,Pd)S series] and sulfarsenides [irarsite (IrAsS) – hollingworthite (RhAsS) series], (2) to characterize notable compositional features of these PGM, with emphasis on the distribution and behavior of minor and trace elements, and (3) to discuss the genetic and crystallochemical implications, some of which extend our knowledge on these economically important species of PGM.

Occurrence and Associated Minerals

The Kirakkajuppura PGE deposit is located near the interface between ultramafic and gabbroic cumulates, close to the contact with the country rocks at the northern end of the Penikat complex (Alapieti & Lahtinen 1986, 1989, Halkoaho *et al.* 1990, Alapieti & Halkoaho 1995). In this deposit, the PGE mineralization is associated with hydrous magnesian silicates, accessory chromite, minor chalcopyrite, bornite, millerite, and secondary chalcocite (Barkov *et al.* 1999a). The principal PGM at Kirakkajuppura are vysotskite – braggite, zvyagintsevite (Pd_3Pb), an unnamed Pd–Pb oxide ($Pd^{2+}{}_7Pb^{2+}O_8$) formed at the expense of zvyagintsevite, and various PGE-rich thiospinels, members of the cuprorhodsite – ferrorhodsite – malanite series: $^{A}(Cu^{+})^{B}[Rh^{3+}(Pt,Ir)^{4+}]S^{2-}{}_4$ – $^{A}(Fe^{3+}{}_{0.5}Cu^{+}{}_{0.5})^{B}Rh^{3+}{}_2S^{2-}{}_4$ (Barkov *et al.* 1999a, 2000). Typically, nearly all sulfur in the PGE-rich, BMS-poor samples is accounted by the PGE sulfide species, mainly vysotskite (Barkov *et al.* 1999a). The other PGM and PGE-rich phases observed in the Kirakkajuppura deposit are laflammeite, laurite – erlichmanite, irarsite – hollingworthite, keithconnite, a Pb-rich phase [$Pd_{20}(Te_6Pb)_7$] likely related to keithconnite, unnamed $Rh(Ni,Fe,Cu)_2S_3$, (Pd,Pt)Cu (the Pd-dominant analogue of hongshiite?), palladoan gold (up to 9 wt.% Pd), and a series of unusual Fe–Pb–Cu–PGE-rich chalcogenides, which are related to konderite (Barkov *et al.* 2004a).

Analytical Method, Color X-Ray Maps and Electron-Microprobe Profiles

The electron-microprobe data were obtained by wavelength-dispersion spectrometry (WDS) using a fully automated JEOL JXA–8900 electron microprobe operated at 20 kV and 30 nA. A finely focused beam and the following X-ray lines and set of standards were used: Ru*L*α, Os*L*α, Ir*L*α, Rh*L*α, Pt*L*α, Pd*L*β (pure Ru, Os, Ir, Rh, Pt, and Pd), Fe*K*α (FeS_2), Ni*K*α, Co*K*α (CoNiAs), Cr*K*α (chromite), Pb*M*α (PbS), S*K*α (PbS), and As*L*β ($PtAs_2$). The raw data were processed and corrected on-line using the ZAF (JEOL) and CTZ programs. The minimum limits of detection were 0.02 wt.% for S, 0.03 wt.% for Fe and Co, 0.04 wt.% for Ni and Cr, 0.08 wt.% for Rh, and 0.09 wt.% for Ru and As.

We used detailed electron-microprobe profiles (WDS), done in automatic mode, in order to characterize zoning and compositional variations in the PGE sulfides and sulfarsenides. A step interval of 1 μm was chosen for the profiles *ab*, *cd*, and *ef* of Figures 1 to 3, because of the presence of very narrow zones (*e.g.*, Fig. 3B). A few point analyses made at the contact of the PGE sulfides with the sulfarsenides were omitted in order to avoid possible contamination. Also, we used color X-ray mapping in order to document the fine-scale zoning and the distribution of major and minor elements. The zones with the highest concentration of an element appear white, followed by red, orange, yellow, green, blue, dark blue, and zones with the lowest concentration are violet (Figs. 1 to 3).

Zoning in Laurite – Erlichmanite

Laurite – erlichmanite (hereafter Lrt–Erl) occurs as (1) individual and notably zoned crystals (Fig. 1), (2) cores of complexly zoned grains (Figs. 2, 3), which are mantled by irarsite – hollingworthite (hereafter Irs–Hlw), and (3) large and euhedral grains with a slight or irregular zoning (Figs. 4A, B). It is noteworthy that individual grains of Lrt–Erl at Kirakkajuppura may reach 0.3 mm in size, and these are much larger than grains of Lrt–Erl observed in other PGE deposits associated with layered intrusions.

Electron-microprobe profile "ab"

The zoned crystal of Lrt–Erl shown in Figures 1A–D consists of a euhedral core, most faces of which are subparallel to the crystal edges. The core itself is zoned and contains three Os-enriched zones (see white and red zones shown in Fig. 1B). The X-ray maps for Ir and As are nearly identical (*cf.* Figs. 1C, D), indicative of a close relationship between these two elements. Results obtained for the profile *ab* across the zoned Lrt–Erl crystal (Fig. 1, Tables 1, 2) reveal sympathetic covariations of Ir (Fig. 5A), Rh, As (Fig. 5B), and Fe (Fig. 5C). Anticorrelation of Ru and Ir is observed in the area of analysis no. 40 (Fig. 5A), consistent with an Ir-for-Ru

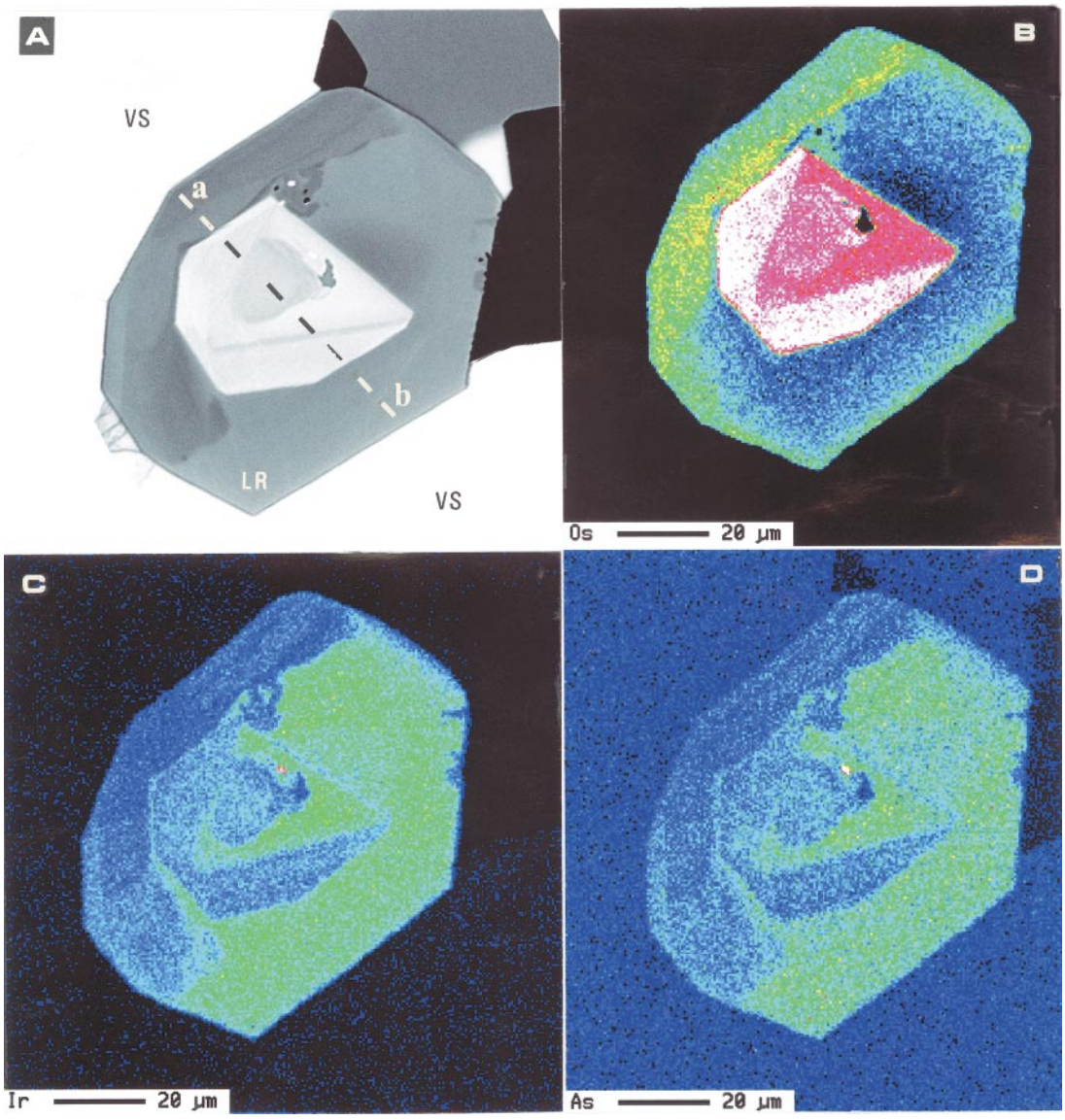

FIG. 1. A. Back-scattered electron (BSE) image of a euhedral grain of zoned laurite – erlichmanite (LR), which is enclosed by vysotskite – braggite [$(Pd_{0.58-0.61}Pt_{0.39-0.36}Ni_{0.01})_{\Sigma 1.01-1.02}S_{1.01-1.02}$] (VS). B–D: Color X-ray maps showing the distribution of Os (B), Ir (C), and As (D) in this zoned grain. Variations in contents of elements are shown by the change in color (white is the highest, followed by red, orange, yellow, green, blue, dark blue, and violet, which is the lowest). The dashed line (*ab*) shows the location of electron-microprobe profile. The scale bar (Fig. 1B) is 20 µm.

tion with S (R = –0.94), and correlates positively with both Rh and Fe (R = 0.89 and 0.96, respectively). Iron correlates positively with As (R = 0.95; Fig. 6B) and negatively with S (R = –0.89). Also, the Rh–As and Rh–Fe correlations are positive (R = 0.90 and 0.83, respectively), and the Rh–S correlation is negative (R = –0.84). The strong interrelationships of Ir, Rh, and Fe with As are also demonstrated by a nearly perfect positive correlation between (Ir + Rh + Fe) and As (R = 0.99; Fig. 6C).

The minor Pt content in Lrt–Erl (Fig. 1A) increases toward the grain boundaries with the host vysotskite – braggite [$(Pd_{0.58–0.61}Pt_{0.39–0.36}Ni_{0.01})_{\Sigma 1.01–1.02}S_{1.01–1.02}$]; this effect is interpreted to be due to fluorescence interference from the host vysotskite – braggite. The contrasting behavior of Pt and Pd here (Tables 1, 2) is apparently due to the difference in the respective value of fluorescent yield, which is much greater for Pt than for Pd (J.H.G. Laflamme, writ. commun.).

Electron-microprobe profile "cd"

The Lrt–Erl core of this composite grain is cryptically zoned with respect to Os, Ru, Ir, As and S (Tables 3, 4, Figs. 2A–F), and is mantled by a zoned Irs–Hlw, which is characterized below. Very narrow compositional zones are present in this Lrt–Erl, as is well illustrated in the X-ray map for Os (Fig. 2B). The content of Os generally decreases and that of Ru increases toward the grain edge (Figs. 2B, D, 7A), and the Ru–Os correlation is negative (R = –0.90; n = 74). Iridium and Rh vary sympathetically (Fig. 7B). Values of the *ir#* index [*i.e.*, 100 Ir / (Ir + Rh), Ir and Rh in *apfu*] vary slightly within the Lrt–Erl core (Fig. 7C).

The content of Fe in Lrt–Erl is higher than in the associated Irs–Hlw. Iron is distributed rather heterogeneously, and the Fe content generally increases toward the grain margin, in common with Ru and in contrast with Os (*cf.* Figs. 7D, A). Elevated levels of As are observed locally (Fig. 7E). Iridium correlates positively with As and Rh (R = 0.97 for both As and Rh: Figs. 8A, B) and negatively with S (R = –0.96; Fig. 8C). The Ir–Ru and Rh–Ru correlations are negative (R = –0.63 and –0.69, respectively; n = 74), whereas the Ir–Os and Rh–Os correlations are weakly positive (R = 0.24 and 0.32, respectively). Thus, Ir and Rh likely replace Ru rather than Os. The behavior of Rh is uniform with that of Ir; the Rh–As correlation is strongly positive (R = 0.95), and the Rh–S correlation is negative (R = –0.93). Arsenic is anticorrelated with S (R = –0.99; Fig. 8D), indicative of the As-for-S substitution.

In the *cd* profile, Fe correlates positively with Ru (R = 0.91; n = 74), negatively with Os (R = –0.94), slightly negatively with As (R = –0.54) and positively with S (R = 0.56), but there is no well-defined correlation with either Ir or Rh. These relationships are in contrast with those observed for Fe in the *ab* profile.

Electron-microprobe profile "ef"

The Lrt–Erl series forms a large core in a polymineralic grain of PGM, which is roundish in shape (Fig. 3A) and mantled by Irs–Hlw (see a description below), in common with the texture shown in Figure 2A. Cuprorhodsite [$Cu(Rh,Pt)_2S_4$] and a complex konderite-type chalcogenide(s) rich in Fe, Pb, Cu, Rh, Pd, and Ir occurs at the margin (Fig. 3A).

The Lrt–Erl core is about 0.1 mm in size and complexly zoned, consisting of individual microzones shown on the X-ray map for Os (Fig. 3B). The presence of an internal zone (*ca.* 25 μm in size: "white" in Fig. 3B) in the center of the larger euhedral "core" (*ca.* 50 μm: red in Fig. 3B) is noteworthy. Variations in Ru are mainly responsible for the observed "rhythmic" zoning (Fig. 9A), with a maximum Ru content similar to that of the Lrt–Erl grains shown in Figures 1 and 2 (up to *ca.* 0.7 Ru *apfu*). In addition, there are also microzones enriched in Ir and As in the Lrt–Erl core, with nearly identical patterns of distribution (Figs. 3C, D), again indicative of a strong relationship between Ir and As. Also, a strong enrichment in Ru relative to Os is characteristic (Fig. 9A).

Iridium and Rh vary sympathetically (Fig. 9B), and values of the *ir#* index are, in general, tightly constrained (Fig. 9C). A heterogeneous distribution of Fe is characteristic (Fig. 9D). A narrow zone in the center is enriched in Fe and is relatively poor in Ru and rich in Os; thus, Fe replaces Ru rather than Os. With the exception of this zone, a general increase in Fe toward the margin is clearly observed. The As-enriched microzones are poorer in S, consistent with As-for-S substitution (Fig. 9E).

The Ir–As correlation (Fig. 10A) is strongly positive in Lrt–Erl (R = 0.98; n = 132); in addition, Ir correlates positively with Rh (R = 0.95) and negatively with S (R = –0.96). Rhodium also displays a positive correlation with As (R = 0.92) and a negative correlation with S (R = –0.91). Neither Ir nor Rh displays a well-defined correlation with Fe. The correlation of (Ir + Rh) and As is strongly positive (R = 0.97; Fig. 10B), and the As–S correlation is nearly inverse (R = –0.98).

Zoning in Irarsite – Hollingworthite

Electron-microprobe profiles "cd" and "ef"

The Irs–Hlw series displays the following characteristics: (1) it occurs as rim-like zones around Lrt–Erl (Figs. 2, 3). (2) It is very poor in Os and is, in contrast, relatively enriched in Ru (*ca.* 0.1 *apfu*: Figs. 7A, 9A, Tables 3 to 6). (3) Also, the compositional trends for Ru and Os are somewhat distinct: the observed decrease in Ru is sharp, whereas Os displays a gradual decrease from Lrt–Erl to the associated Irs–Hlw (Figs. 7A, 9A). (4) It is cryptically zoned, with the Ir content decreas-

ing (and the Rh content increasing) outward. In both cases (*cf.* Figs. 7B, 9B), the maximum content of Ir is close to 0.7 *apfu* (*i.e.,* approximately 70 mol.% IrAsS). (5) Although the contents of Ir and Rh change rapidly (Figs. 7B, 9B), the *ir#* index displays gradual trends (Figs. 7C, 9C), with a general decrease outward, from Lrt–Erl toward the associated Irs–Hlw. (6) The content of Fe in Irs–Hlw is several times less than that in the associated Lrt–Erl (Figs. 7D, 9D). (7) Fe increases toward the margin (Figs. 7D, 9D). (8) Irs–Hlw is characterized by a significant deficit in As and corresponding excess in S (Figs. 7E, 9E, Tables 3 to 6) and thus deviates from the ideal *Me*AsS stoichiometry.

Description of an Unusual Microtexture and Compositions of Slightly Zoned Laurite – Erlichmanite

An unusual texture, hitherto unreported, is shown in Figure 4A: a large crystal of Lrt–Erl (*ca.* 250 μm) contains abundant and globular inclusions of a PGM (bright white) and a hydrous silicate (black: Fig. 4A). Some of these microglobules (shown by the black arrows: Fig. 4A) are composed of both phases [PGM and hydrous silicate(s)], separated by a straight and uniformly oriented phase-boundary. Results of quantitative energy-dispersion (EDS) electron-microprobe analyses indicate that this PGM is an intermetallic compound of Pd and Pb, having the following composition: Pd 59.92, Pb 40.08, total 100.0 wt.%. The formula is $Pd_{2.98}Pb_{1.02}$, indicative of zvyagintsevite (Pd_3Pb), which is a very rare species in other localities but quite common at Kirakkajuppura (Barkov *et al.* 1999a). The hydrous silicate is clinochlore with the following composition (EDS data, in wt.%): SiO_2 25.30, Al_2O_3 21.16, Cr_2O_3 0.60, FeO 17.06, MnO 0.31, MgO 21.32, Na_2O 0.43 (K, Ca, Ti, Ni and Cl were sought, but not detected). The formula is $[(Mg_{3.29}Fe_{1.47}Al_{0.25}Na_{0.09}Mn_{0.03})_{\Sigma 5.13}Al_{1.00}(Si_{2.62}Al_{1.33}Cr_{0.05})_{\Sigma 4.00}O_{10}(OH)_8]$ (O = 14); the *mg#* value [*i.e.*, 100 Mg / (Mg + Fe + Mn)] is 69.

The Lrt–Erl grain hosting the microglobules exhibits a slight zoning, with the following ranges of composition (in *apfu*): Ru 0.62–0.70, Os 0.22–0.28, Ir 0.04–0.06, and Rh 0.01–0.02 (Table 7), and a zone enriched in Ru occurs at the margin (gray: Fig. 4A). In addition, a total of ninety WDS analyses were made on

TABLE 1. COMPOSITIONS OF ZONED LAURITE–ERLICHMANITE (PROFILE *ab*) FROM THE PENIKAT LAYERED COMPLEX, FINLAND

	Ru	Os	Ir	Rh	Pt	Pd	Fe	Ni	As	S	Total
1	34.30	25.31	4.01	0.69	0.69	0.06	0.22	0.05	0.40	32.75	98.48
2	34.02	25.57	3.88	0.75	0.68	0.18	0.23	0.02	0.44	32.98	98.75
3	33.95	26.25	4.10	0.80	0.39	0.07	0.22	0.02	0.47	32.00	98.27
4	32.71	26.93	4.03	0.69	0.41	0.13	0.21	0.03	0.48	32.67	98.29
5	32.51	27.31	4.43	0.75	0.33	n.d.	0.22	0.01	0.52	32.61	98.69
6	32.72	27.23	4.42	0.62	0.34	0.16	0.22	0.04	0.51	31.87	98.13
7	32.30	27.13	4.65	0.82	0.16	0.08	0.23	0.01	0.63	31.87	97.88
8	19.86	39.84	6.22	1.31	0.32	0.11	0.26	0.05	0.95	28.84	97.76
9	21.61	37.65	6.54	1.36	0.25	n.d.	0.26	0.06	0.97	29.33	98.03
10	21.54	37.44	6.65	1.41	0.31	0.11	0.28	0.04	1.00	29.74	98.52
11	21.59	37.45	6.73	1.34	0.16	0.15	0.28	0.03	0.89	29.66	98.28
12	21.45	37.44	6.85	1.34	0.23	n.d.	0.26	0.05	1.02	29.53	98.17
13	22.70	35.01	7.26	1.38	0.11	0.13	0.29	0.04	1.25	29.45	97.62
14	22.91	34.92	7.42	1.45	0.16	0.06	0.30	0.03	1.25	29.48	97.98
15	22.99	34.76	7.63	1.33	0.05	0.08	0.28	0.07	1.24	29.49	97.92
16	22.56	34.76	7.67	1.53	0.09	0.12	0.29	0.02	1.27	29.26	97.57
17	22.70	35.09	7.73	1.32	0.15	0.12	0.29	0.03	1.37	29.51	98.31
18	22.91	34.73	7.72	1.48	0.03	n.d.	0.27	0.04	1.33	29.38	97.89
19	23.70	35.23	6.49	1.17	0.11	0.04	0.25	0.04	0.99	29.85	97.87
20	21.76	34.29	8.50	1.88	n.d.	0.02	0.32	0.06	1.55	29.15	97.53
21	19.92	33.21	11.58	2.37	n.d.	n.d.	0.38	0.06	2.02	28.78	98.32
22	19.14	32.59	12.20	2.70	n.d.	n.d.	0.38	0.09	2.40	28.58	98.08
23	19.10	32.71	12.06	2.74	0.03	0.05	0.35	0.08	2.31	28.65	98.08
24	19.39	32.75	11.56	2.72	0.01	0.22	0.34	0.08	2.26	28.46	97.79
25	20.73	33.07	10.70	2.44	n.d.	n.d.	0.31	0.05	2.08	29.05	98.43
26	21.94	33.79	8.50	2.03	0.13	0.06	0.27	0.07	1.59	28.99	97.37
27	23.08	35.54	6.73	1.51	0.13	n.d.	0.26	0.07	1.17	29.30	97.79
28	21.71	37.75	6.56	1.45	0.10	n.d.	0.24	0.03	0.99	29.10	97.93
29	21.47	37.35	6.51	1.41	0.17	n.d.	0.25	0.05	0.98	29.08	97.27
30	25.31	29.69	8.83	1.66	0.09	0.14	0.32	0.07	1.53	29.46	97.10
31	30.98	19.24	12.29	1.83	0.11	n.d.	0.40	0.06	2.18	30.87	97.96
32	30.76	19.69	12.20	1.96	0.20	n.d.	0.39	0.07	2.24	31.10	98.61
33	30.44	20.35	11.83	1.85	0.16	0.12	0.36	0.09	2.22	30.21	97.63
34	30.11	20.25	11.94	1.96	0.28	n.d.	0.40	0.06	2.29	30.69	97.98
35	29.92	20.57	12.03	2.06	0.22	0.01	0.37	0.08	2.25	30.10	97.61
36	29.63	21.14	11.74	1.77	0.36	0.02	0.37	0.05	2.22	30.47	97.77
37	29.05	21.45	11.64	1.90	0.50	0.04	0.36	0.06	2.17	30.50	97.67
38	28.97	22.12	11.57	1.83	0.84	n.d.	0.36	0.06	2.12	29.94	97.81
39	28.54	22.85	11.03	1.78	0.92	n.d.	0.36	0.07	2.11	30.16	97.82
40	28.09	23.82	10.61	1.63	1.08	0.07	0.33	0.08	2.00	29.89	97.60

The results of these electron-microprobe analyses (WDS), from 1 to 40, are representative of the profile *ab* (Fig. 1A); they are listed (in wt.%) in order from the point *a* to the point *b*. Results of the entire set of analyses obtained in the profile *ab* are presented in Figures 5A to 6C. The presence of minor Pt at the margin of this grain is ascribed to interference from the host vysotskite–braggite (Fig. 1A).

TABLE 2. ATOM PROPORTIONS IN ZONED LAURITE–ERLICHMANITE (PROFILE *ab*) FROM THE PENIKAT LAYERED COMPLEX, FINLAND

	Ru	Os	Ir	Rh	Pt	Pd	Fe	Ni	*Me*	As	S	As+S
1	0.66	0.26	0.041	0.013	0.007	0.001	0.008	0.002	0.99	0.010	2.00	2.01
2	0.65	0.26	0.039	0.014	0.007	0.003	0.008	0.001	0.98	0.011	2.00	2.01
3	0.67	0.27	0.042	0.015	0.004	0.001	0.008	0.001	1.01	0.012	1.98	1.99
4	0.64	0.28	0.041	0.013	0.004	0.002	0.007	0.001	0.99	0.013	2.00	2.01
5	0.63	0.28	0.045	0.014	0.003	-	0.008	<0.001	0.98	0.014	2.00	2.01
6	0.65	0.29	0.046	0.012	0.003	0.003	0.008	0.001	1.01	0.014	1.98	1.99
7	0.64	0.28	0.048	0.016	0.002	0.002	0.008	<0.001	1.00	0.017	1.98	2.00
8	0.43	0.46	0.071	0.028	0.004	0.002	0.010	0.002	1.01	0.028	1.97	2.00
9	0.46	0.43	0.073	0.028	0.003	-	0.010	0.002	1.01	0.028	1.97	2.00
10	0.45	0.42	0.074	0.029	0.003	0.002	0.011	0.001	0.99	0.028	1.98	2.01
11	0.46	0.42	0.075	0.028	0.002	0.003	0.011	0.001	1.00	0.025	1.98	2.01
12	0.46	0.42	0.076	0.028	0.003	-	0.010	0.002	1.00	0.029	1.97	2.00
13	0.48	0.39	0.081	0.029	0.001	0.003	0.011	0.001	1.00	0.036	1.96	2.00
14	0.48	0.39	0.082	0.030	0.002	0.001	0.011	0.001	1.00	0.036	1.96	2.00
15	0.49	0.39	0.085	0.028	<0.001	0.002	0.011	0.003	1.01	0.035	1.96	2.00
16	0.48	0.39	0.086	0.032	0.001	0.002	0.011	<0.001	1.00	0.036	1.96	2.00
17	0.48	0.39	0.086	0.027	0.002	0.002	0.011	0.001	1.00	0.039	1.96	2.00
18	0.48	0.39	0.086	0.031	<0.001	-	0.010	0.001	1.00	0.038	1.96	2.00
19	0.50	0.39	0.072	0.024	0.001	0.001	0.009	0.001	1.00	0.028	1.97	2.00
20	0.46	0.39	0.095	0.039	-	<0.001	0.012	0.002	1.00	0.044	1.96	2.00
21	0.43	0.38	0.130	0.050	-	-	0.015	0.002	1.01	0.058	1.94	2.00
22	0.41	0.37	0.138	0.057	-	-	0.015	0.003	0.99	0.070	1.93	2.00
23	0.41	0.37	0.136	0.058	<0.001	0.001	0.014	0.003	0.99	0.067	1.94	2.01
24	0.42	0.37	0.131	0.058	<0.001	0.005	0.013	0.003	1.00	0.066	1.93	2.00
25	0.44	0.37	0.119	0.051	-	-	0.012	0.002	0.99	0.060	1.94	2.00
26	0.47	0.38	0.095	0.043	0.001	0.001	0.010	0.003	1.00	0.046	1.95	2.00
27	0.49	0.40	0.075	0.031	0.001	-	0.010	0.003	1.01	0.033	1.96	1.99
28	0.46	0.43	0.074	0.030	0.001	-	0.009	0.001	1.01	0.029	1.96	1.99
29	0.46	0.43	0.073	0.030	0.002	-	0.010	0.002	1.01	0.028	1.97	2.00
30	0.53	0.33	0.097	0.034	0.001	0.003	0.012	0.003	1.01	0.043	1.95	1.99
31	0.62	0.20	0.129	0.036	0.001	-	0.014	0.002	1.00	0.059	1.94	2.00
32	0.61	0.21	0.127	0.038	0.002	-	0.014	0.002	1.00	0.060	1.94	2.00
33	0.61	0.22	0.126	0.037	0.002	0.002	0.013	0.003	1.01	0.060	1.92	1.98
34	0.60	0.22	0.126	0.039	0.003	-	0.014	0.002	1.00	0.062	1.94	2.00
35	0.61	0.22	0.128	0.041	0.002	<0.001	0.014	0.003	1.02	0.062	1.92	1.98
36	0.60	0.23	0.124	0.035	0.004	<0.001	0.014	0.002	1.01	0.060	1.94	2.00
37	0.59	0.23	0.124	0.038	0.005	<0.001	0.013	0.002	1.00	0.059	1.94	2.00
38	0.59	0.24	0.124	0.037	0.009	-	0.013	0.002	1.02	0.058	1.93	1.99
39	0.58	0.25	0.118	0.036	0.010	-	0.013	0.002	1.01	0.058	1.93	1.99
40	0.58	0.26	0.114	0.033	0.011	0.001	0.012	0.003	1.01	0.055	1.93	1.99

The analytical results (in wt.%) are listed in Table 1; the location of this profile (*ab*) is shown in Figure 1A. The atom proportions are based on three atoms per formula unit.

substitution. In other zones of this crystal, Ir seems to substitute for (Os + Ru) (Fig. 5A). Ruthenium and Os replace each other and are negatively correlated, with the correlation coefficient R of –0.86, based on a total of seventy-two point analyses (hereafter n = 72). Arsenic clearly substitutes for S; thus they are negatively correlated (R = –0.95; Figs. 5B, D).

The behavior of Ir, Rh and Fe is notably uniform (sympathetic). Iridium displays a strong positive correlation with As (R = 0.99; Fig. 6A), a negative correla-

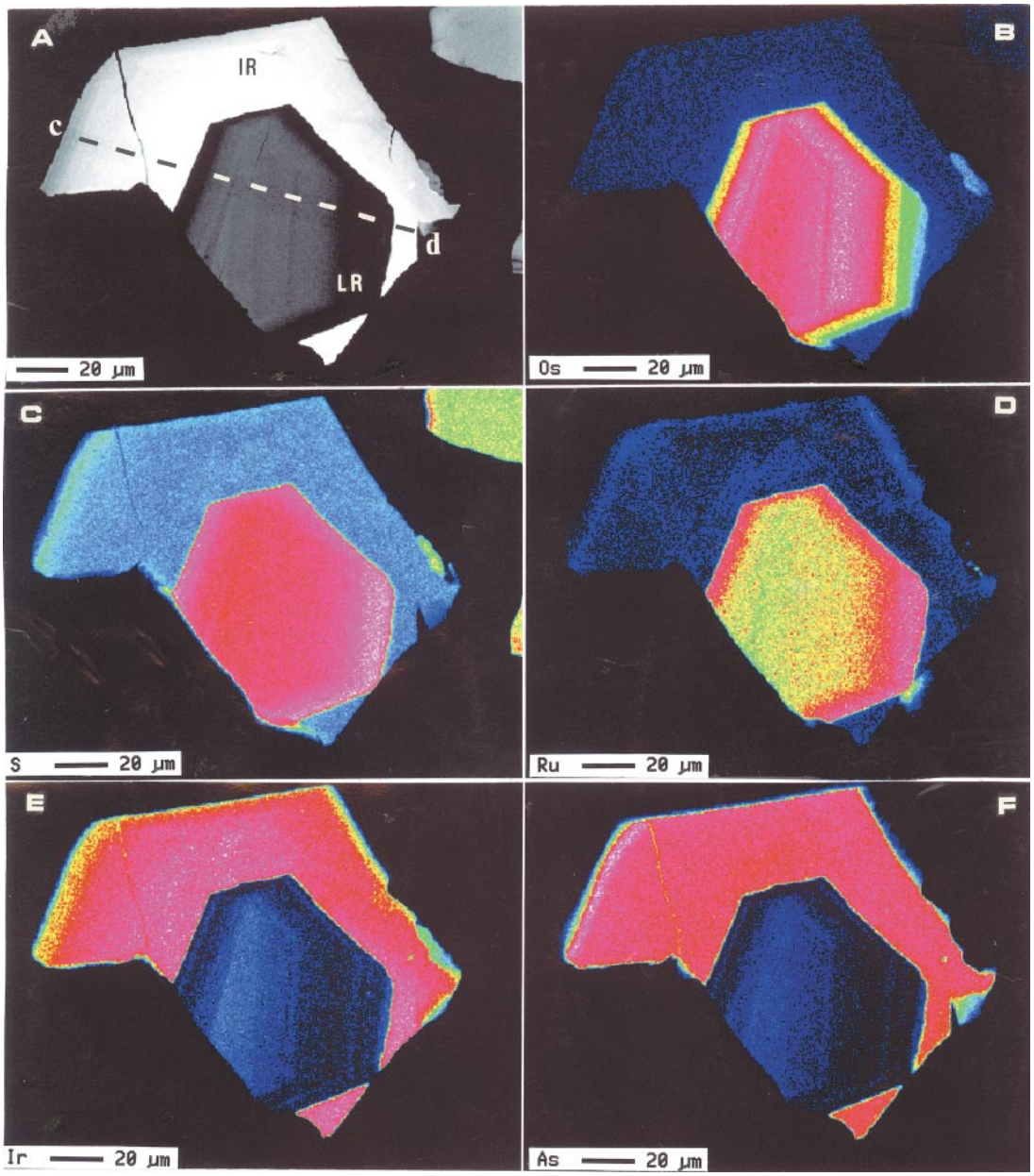

FIG. 2. BSE image (A) and the color X-ray maps showing the distribution of Os (B), S (C), Ru (D), Ir (E), and As (F) in a zoned grain of laurite – erlichmanite (LR) and irarsite – hollingworthite (IR). The surrounding material is epoxy. The location of the electron-microprobe profile (*cd*) is shown by the dashed line in Figure 2A. The scale bar is 20 µm.

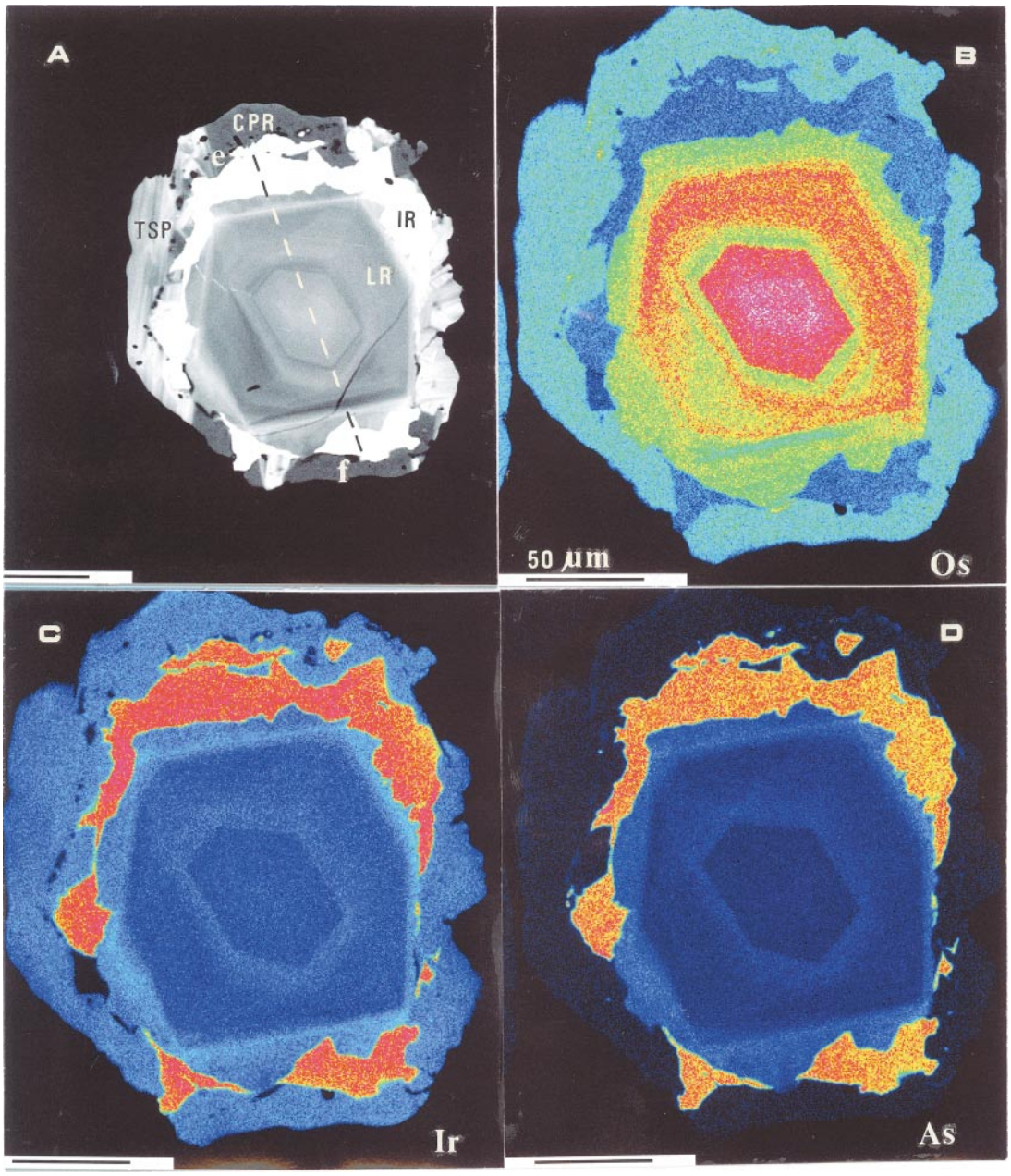

FIG. 3. BSE image of a concentrically zoned grain of various platinum-group minerals (PGM), consisting of laurite – erlichmanite (LR), irarsite – hollingworthite (IR), cuprorhodsite [$Cu(Rh,Pt,Ir)_2S_4$] (CPR) and a Pb–Fe–Cu–PGE-rich PGM related to thiospinels (TSP). The dashed line (*ef*) shows the location of the electron-microprobe profile. The surrounding material is epoxy. B–D. Color X-ray maps showing the distribution of Os (B), Ir (C), and As (D). The scale bar (Fig. 3B) is 50 μm.

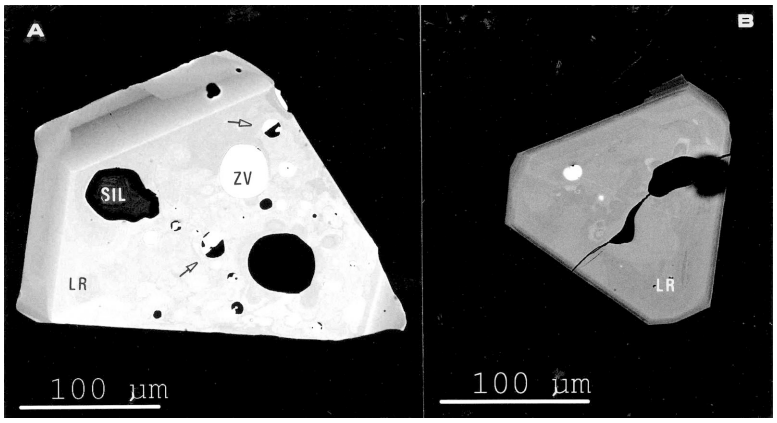

FIG. 4. A. An unusual texture observed in a large grain of laurite – erlichmanite (LR), consisting of abundant, globular inclusions of zvyagintsevite [$Pd_{2.98}Pb_{1.02}$: EDS electron-microprobe data] (ZV: bright white) and a hydrous silicate (*i.e.*, clinochlore: SIL, black). The two-phase microglobules, ZV + SIL, separated by a straight border, are shown by arrows (A). B. A large, euhedral grain of laurite – erlichmanite (LR). The surrounding material is epoxy. A and B: BSE images.

TABLE 3. COMPOSITIONS OF ZONED LAURITE–ERLICHMANITE AND IRARSITE–HOLLINGWORTHITE (PROFILE *cd*) FROM THE PENIKAT COMPLEX, FINLAND

	Ru	Os	Ir	Rh	Pt	Pd	Fe	Ni	As	S	Total
1	2.89	0.15	37.40	18.73	n.d.	n.d.	0.08	0.04	26.31	15.74	101.34
2	2.37	0.06	39.72	16.97	n.d.	n.d.	0.05	0.03	26.05	15.38	100.63
3	2.03	n.d.	42.55	15.22	n.d.	n.d.	0.03	0.04	25.39	14.50	99.76
4	1.92	n.d.	44.41	13.76	n.d.	n.d.	0.03	0.02	25.20	14.47	99.81
5	1.88	0.01	44.66	13.74	n.d.	0.05	0.02	0.03	25.35	14.60	100.34
6	1.82	0.01	45.93	12.70	n.d.	n.d.	n.d.	0.04	25.08	14.59	100.17
7	2.02	0.01	47.14	11.29	n.d.	n.d.	n.d.	0.07	24.78	14.36	99.67
8	2.50	0.25	47.47	10.37	n.d.	n.d.	0.02	0.07	24.35	14.59	99.62
9	2.42	0.12	47.75	10.07	n.d.	0.02	0.01	0.06	24.33	14.69	99.47
10	2.45	0.12	48.49	9.93	n.d.	n.d.	n.d.	0.04	24.29	14.59	99.91
11	2.44	0.09	48.50	9.70	n.d.	n.d.	0.02	0.06	24.30	14.58	99.69
12	2.27	0.19	49.28	9.63	n.d.	n.d.	0.01	0.05	24.23	14.60	100.26
13	2.68	0.24	49.00	9.09	n.d.	n.d.	n.d.	0.05	24.05	14.38	99.49
14	2.35	0.34	49.68	8.68	n.d.	n.d.	n.d.	0.05	24.22	14.38	99.70
15	2.37	0.57	48.77	9.44	n.d.	n.d.	n.d.	0.03	24.17	14.42	99.77
16	2.07	0.89	48.65	8.97	n.d.	n.d.	n.d.	0.03	24.02	14.24	98.87
17	34.63	18.15	9.84	1.49	n.d.	0.08	0.30	0.06	2.32	33.14	100.01
18	30.39	25.97	8.28	1.15	n.d.	0.06	0.21	0.05	1.79	32.32	100.22
19	27.38	28.59	9.03	1.46	n.d.	n.d.	0.19	0.04	2.28	31.25	100.22
20	26.43	26.37	10.74	1.66	n.d.	0.17	0.17	0.02	3.04	30.83	99.43
21	26.15	25.80	11.74	1.80	n.d.	0.09	0.19	n.d.	3.22	30.84	99.83
22	25.24	24.28	13.80	2.31	n.d.	0.09	0.23	0.05	3.62	30.54	100.16
23	25.48	24.43	13.34	2.41	n.d.	0.01	0.22	0.05	3.53	30.56	100.03
24	25.36	24.45	12.97	2.29	n.d.	n.d.	0.23	0.05	3.52	30.56	99.43
25	26.59	24.82	12.09	1.93	0.16	0.03	0.21	0.04	3.26	30.94	100.07
26	27.11	25.45	11.33	2.02	n.d.	0.05	0.20	0.05	3.03	30.89	100.13
27	26.78	26.52	10.60	1.81	n.d.	0.02	0.20	0.05	2.75	31.17	99.90
28	26.99	26.55	10.29	1.79	0.07	0.05	0.19	0.04	2.81	31.07	99.85
29	27.12	27.62	9.61	1.60	0.06	n.d.	0.20	0.04	2.37	31.42	100.04
30	27.32	26.70	10.13	1.67	0.03	n.d.	0.24	0.04	2.60	31.33	100.06
31	27.12	28.78	8.60	1.32	0.17	n.d.	0.19	0.04	1.99	31.66	99.87
32	27.66	28.95	7.94	1.39	0.04	0.25	0.20	0.03	1.75	31.73	99.94
33	28.26	28.13	7.99	1.26	n.d.	0.03	0.22	0.03	1.70	31.89	99.51
34	29.34	27.17	8.08	1.36	0.14	0.17	0.24	0.05	1.62	32.31	100.48
35	30.37	25.74	7.75	1.18	n.d.	0.04	0.26	0.03	1.48	32.39	99.24
36	32.00	24.03	7.62	1.33	0.06	0.07	0.29	0.07	1.38	32.87	99.72
37	33.95	19.22	9.36	1.57	0.05	0.08	0.38	0.08	1.95	33.36	100.00
38	35.87	18.17	8.43	1.38	n.d.	0.10	0.38	0.07	1.50	33.97	99.87
39	38.75	13.45	9.44	1.43	0.12	0.04	0.43	0.07	1.81	34.51	100.05
40	39.83	13.31	8.56	1.21	0.08	0.14	0.42	0.06	1.39	35.02	100.02
41	2.12	0.53	50.22	8.23	n.d.	n.d.	0.01	0.02	23.70	14.25	99.08
42	2.05	0.47	50.69	8.36	n.d.	0.06	0.01	0.04	23.71	14.26	99.65
43	2.19	0.44	49.93	8.65	n.d.	n.d.	0.01	0.03	23.75	14.21	99.21
44	2.07	0.30	50.30	8.32	n.d.	n.d.	0.01	0.04	23.40	14.28	98.72
45	2.30	0.44	49.16	8.87	n.d.	0.11	0.03	0.03	23.25	14.26	98.45

The results of these WDS analyses, from 1 to 45, are representative of the profile *cd* (Fig. 2A); they are listed (in wt.%) in order from the point *c* to the point *d*. Numbers 1–16 and 41–45: irarsite–hollingworthite. Numbers 17–40: laurite–erlichmanite. Results of the entire set of analyses obtained in the profile *cd* are presented in Figures 7A to 8D.

TABLE 4. ATOM PROPORTIONS OF ZONED LAURITE–ERLICHMANITE AND IRARSITE- HOLLINGWORTHITE (PROFILE *cd*), PENIKAT COMPLEX, FINLAND

	Ru	Os	Ir	Rh	Pt	Pd	Fe	Ni	*Me*	As	S	As+S
1	0.07	0.002	0.467	0.437	-	-	0.003	0.002	0.98	0.84	1.18	2.02
2	0.06	0.001	0.506	0.404	-	-	0.002	0.001	0.97	0.85	1.18	2.03
3	0.05	0	0.562	0.376	-	-	0.001	0.002	0.99	0.86	1.15	2.01
4	0.05	0	0.591	0.342	-	-	0.001	0.001	0.98	0.86	1.15	2.01
5	0.05	<0.001	0.591	0.340	-	0.001	0.001	0.001	0.98	0.86	1.16	2.02
6	0.05	<0.001	0.612	0.316	-	-	-	0.002	0.98	0.86	1.17	2.03
7	0.05	<0.001	0.637	0.285	-	-	-	0.003	0.98	0.86	1.16	2.02
8	0.06	0.003	0.641	0.262	-	-	0.001	0.003	0.97	0.84	1.18	2.02
9	0.06	0.002	0.645	0.254	-	<0.001	<0.001	0.002	0.97	0.84	1.19	2.03
10	0.06	0.002	0.656	0.251	-	-	-	0.002	0.97	0.84	1.18	2.02
11	0.06	0.001	0.657	0.246	-	-	0.001	0.002	0.97	0.85	1.18	2.03
12	0.06	0.003	0.667	0.243	-	-	<0.001	0.002	0.97	0.84	1.18	2.02
13	0.07	0.003	0.670	0.232	-	-	-	0.002	0.98	0.84	1.18	2.02
14	0.06	0.005	0.680	0.222	-	-	-	0.002	0.97	0.85	1.18	2.03
15	0.06	0.008	0.665	0.240	-	-	-	0.001	0.98	0.85	1.18	2.03
16	0.05	0.012	0.672	0.231	-	-	-	0.001	0.97	0.85	1.18	2.03
17	0.65	0.18	0.097	0.028	-	0.001	0.010	0.002	0.97	0.059	1.97	2.03
18	0.59	0.27	0.085	0.022	-	0.001	0.007	0.002	0.97	0.047	1.98	2.03
19	0.54	0.30	0.094	0.029	-	-	0.007	0.001	0.98	0.061	1.96	2.02
20	0.53	0.28	0.113	0.033	-	0.003	0.006	0.001	0.97	0.082	1.95	2.03
21	0.52	0.27	0.124	0.035	-	0.002	0.007	0	0.97	0.087	1.95	2.04
22	0.51	0.26	0.146	0.046	-	0.002	0.008	0.002	0.97	0.098	1.93	2.03
23	0.51	0.26	0.141	0.048	-	<0.001	0.008	0.002	0.97	0.096	1.93	2.03
24	0.51	0.26	0.137	0.045	-	-	0.008	0.002	0.96	0.096	1.94	2.04
25	0.53	0.26	0.127	0.038	0.002	<0.001	0.007	0.001	0.97	0.088	1.94	2.03
26	0.54	0.27	0.119	0.039	-	0.001	0.007	0.002	0.98	0.081	1.94	2.02
27	0.53	0.28	0.111	0.035	-	<0.001	0.007	0.002	0.97	0.074	1.96	2.03
28	0.54	0.28	0.108	0.035	0.001	0.001	0.007	0.001	0.97	0.076	1.95	2.03
29	0.54	0.29	0.100	0.031	0.001	-	0.007	0.001	0.97	0.063	1.97	2.03
30	0.54	0.28	0.106	0.033	<0.001	-	0.009	0.001	0.97	0.070	1.96	2.03
31	0.54	0.30	0.090	0.026	0.002	-	0.007	0.001	0.97	0.053	1.98	2.03
32	0.55	0.30	0.083	0.027	<0.001	0.005	0.007	0.001	0.97	0.047	1.98	2.03
33	0.56	0.30	0.083	0.024	-	<0.001	0.008	0.001	0.97	0.045	1.98	2.03
34	0.57	0.28	0.083	0.026	0.001	0.003	0.009	0.002	0.98	0.043	1.98	2.02
35	0.59	0.27	0.079	0.023	-	0.001	0.009	0.001	0.97	0.039	1.99	2.03
36	0.61	0.25	0.077	0.025	<0.001	0.001	0.010	0.002	0.98	0.036	1.99	2.03
37	0.64	0.19	0.093	0.029	<0.001	0.001	0.013	0.003	0.97	0.050	1.98	2.03
38	0.67	0.18	0.082	0.025	-	0.002	0.013	0.002	0.97	0.038	1.99	2.03
39	0.71	0.13	0.091	0.026	0.001	<0.001	0.014	0.002	0.97	0.045	1.98	2.03
40	0.72	0.13	0.081	0.022	0.001	0.002	0.014	0.002	0.97	0.034	2.00	2.03
41	0.06	0.007	0.696	0.213	-	-	<0.001	0.001	0.97	0.84	1.18	2.02
42	0.05	0.007	0.700	0.216	-	0.001	<0.001	0.002	0.98	0.84	1.18	2.02
43	0.06	0.006	0.690	0.223	-	-	<0.001	0.001	0.98	0.84	1.18	2.02
44	0.05	0.004	0.699	0.216	-	-	<0.001	0.002	0.98	0.83	1.19	2.02
45	0.06	0.006	0.683	0.230	-	0.003	0.001	0.001	0.98	0.83	1.19	2.02

The analytical results (in wt.%) are listed in Table 3 (profile *cd*: Fig. 2A). Numbers 1–16 and 41–45: irarsite–hollingworthite; numbers 17–40: laurite–erlichmanite. The atom proportions are based on three atoms per formula unit.

another large grain of Lrt–Erl (Fig. 4B). The average content and the observed ranges (in wt.%) are: Ru 32.40 (31.35–37.79), Os 29.06 (22.90–30.83), Ir 3.02 (2.42–4.70), Rh 0.81 (0.56–1.28), Pt 0.05 (n.d.–0.23), Fe 0.28 (0.20–0.55), Pd 0.05 (n.d.–0.30), Ni 0.04 (n.d.–0.08), As 0.0 (<0.09), S 33.85 (33.15–34.91), for a total of 99.56 wt.%. The corresponding ranges in *apfu* are: Ru 0.60–0.70, Os 0.22–0.31, Ir 0.02–0.05, Rh 0.01–0.02,

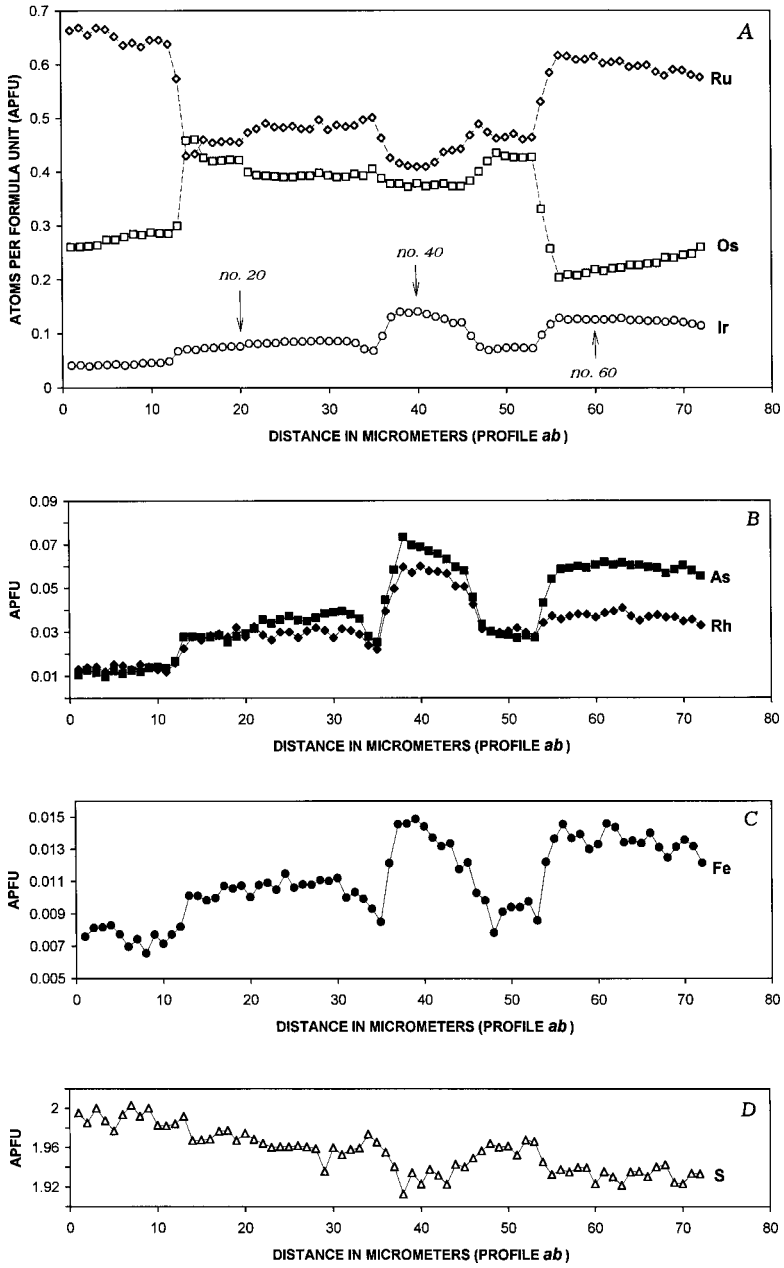

FIG. 5. Variations in concentrations of Ru, Os, Ir (A), Rh, As (B), Fe (C), and S (D), expressed in terms of atoms per formula unit (*apfu*: Σatoms = 3), along electron-microprobe profile *ab* across the zoned grain shown in Figure 1A.

Pt <0.01, Fe <0.01–0.02, Pd <0.01, Ni <0.01, As <0.01, and S 2.01–2.04; the mean composition corresponds to the formula $(Ru_{0.62}Os_{0.29}Ir_{0.03}Rh_{0.015}Fe_{0.01})_{\Sigma 0.97}S_{2.03}$.

Zoning in Vysotskite – Braggite

Individual grains of vysotskite – braggite (hereafter Vsk–Brg) at Kirakkajuppura reach 0.3–0.5 mm in the longest dimension (*e.g.*, Fig. 11). In this deposit, the Vsk–Brg is commonly rich in Pd, poorer in Pt and very poor in Ni, and may occur as unusually long (up to about *ca.* 1 cm) mega-aggregates associated with hydrous magnesian silicates (Barkov *et al.* 1999a).

Zones having a lower average atomic number (gray) are developed within grains of Vsk–Brg (Figs. 11A–C); they have irregular and diffuse boundaries with the host Vsk–Brg and are intimately associated with abundant micro-aggregates of a hydrous silicate(s). Bands of

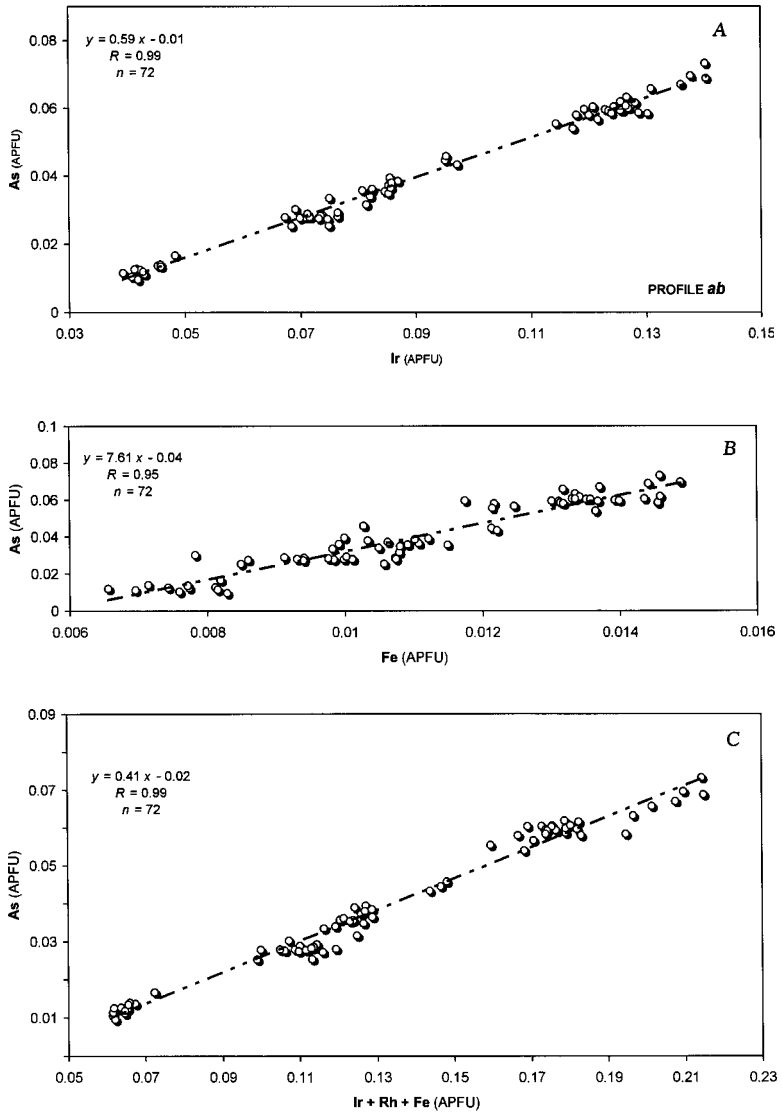

FIG. 6. Correlations of Ir and As (A), Fe and As (B), and (Ir + Rh + Fe) and As (C) (in *apfu*; Σatoms = 3) in compositions of the zoned laurite – erlichmanite from the Penikat complex. Results of 72 WDS analyses, which refer to the profile *ab*, are plotted; the location of this profile is shown in Figure 1A.

submicrometric grains of a hydrous silicate(s) are present in these late-stage Vsk–Brg zones; these bands may be subparallel to each other (black: Figs. 11A–C, 12D). Micro-inclusions of amphibole (rich in Cl) are also abundant in some PGM from Lukkulaisvaara, which is a neighboring layered intrusion in the Fennoscandian Shield (Barkov *et al.* 2004b).

The late zones of the Vsk–Brg are richer in Pd (*i.e.*, in the end-member vysotskite) and, to a lesser degree, in Ni, and are considerably poorer in Pt (*i.e.*, in the

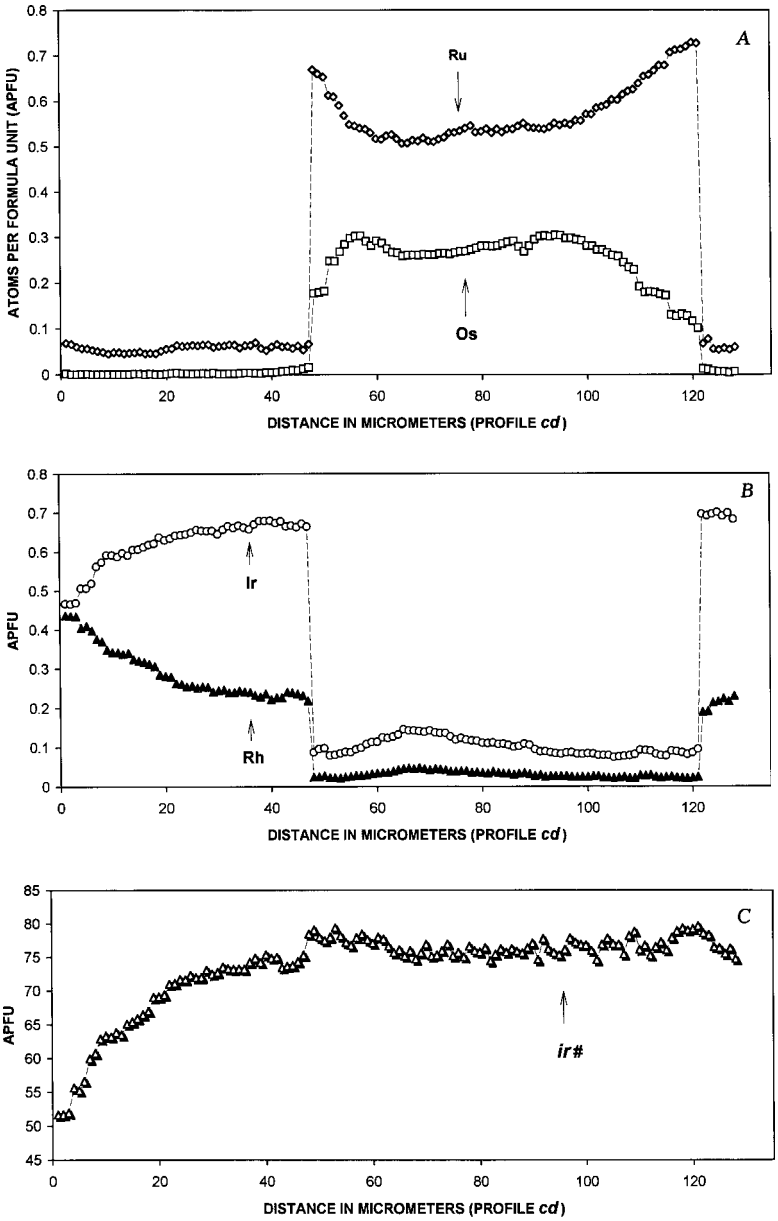

FIG. 7. Variations in content of Ru, Os (A), Rh, Ir (B), Fe (D), S and As (E), and values of the *ir*# index [*i.e.*, 100 Ir / (Ir + Rh)] (C), expressed in *apfu*: Σatoms = 3, along electron-microprobe profile *cd* across the zoned grain shown in Figure 2A.

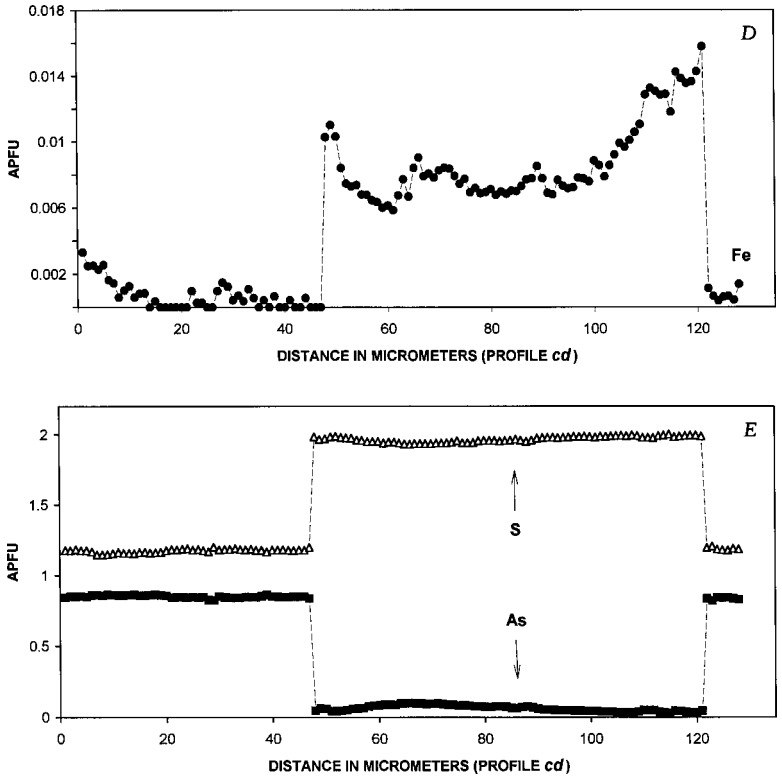

braggite component) than the host Vsk–Brg (*cf.* Table 7, Figs. 12 A–C, 13). We support the recent nomenclature of Cabri (2002), who defined vysotskite as the Pd-dominant member and braggite as the Pt-dominant member of the Vsk–Brg series, in accordance with the "50%" rule of the International Mineralogical Association.

Discussion, Implications and Conclusions

Incorporation of Ir in laurite – erlichmanite and limit of solid solution from (Ru,Os)S_2 toward "$Ir_{1-x}S_2$"

Our results are consistent with three charge-balance mechanisms for the incorporation of Ir in Lrt–Erl. Laurite (and its synthetic analogue: RuS_2) and erlichmanite (OsS_2) are isostructural and have a pyrite-type structure, consistent with the the formal oxidation state 2+ for Ru and Os and the presence of $(S_2)^{2-}$ dumbbells (*e.g.*, Hulliger 1964, Wood & Strens 1979, Bowles *et al.* 1983, Holzwarth *et al.* 1985, Lutz *et al.* 1990, Stingl *et al.* 1992, Colell *et al.* 1994, Schuler *et al.* 1997).

(1) The presence of a limited solid-solution between Lrt–Erl and Irs–Hlw is indicated by the composition profiles *cd* and *ef* (Figs. 8A–D, 10A, B). Iridium is closely associated with Rh and is likely incorporated *via* the following substitution scheme: $[(Ir + Rh)^{3+} + (AsS)^{3-} = (Ru + Os)^{2+} + (S_2)^{2-}]$.

(2) The composition profile *ab* (Figs. 5A–6C) and the X-ray maps (Figs. 1C, D) indicate that As clearly exerts a structural control over the incorporation of Ir, Rh and Fe, which are uniform in behavior; their sum (Ir + Rh + Fe) displays a positive linear correlation with As ($R = 0.99$: $n = 72$). However, in contrast to the solid solution of Lrt–Erl and Irs–Hlw (charge-balance scheme 1), the observed slope is not consistent with (Ir,Rh, Fe)AsS, but indicates a significant deficit in As (Fig. 6C). Thus, it could be instead a solid solution toward an arsenosulfide of the type $Me(S,As)_2$, with the approximate ratio (Ir + Rh + Fe):As of 2.5:1. The excess amount of S, relative to that given by the charge-balance scheme (1), is thus likely required in order to maintain electroneutrality.

(3) Some of the Lrt–Erl grains examined (Figs. 4A, B, Table 7) are essentially devoid of As. Thus, their elevated levels of Ir (up to 5.75 wt.% or 0.06 Ir *apfu*) must have been incorporated in the form of a sulfide component instead of a sulfarsenide. Munson (1968) reported the existence of a pyrite-type IrS_2 phase (*i.e.*, $IrS_{1.9}$ with *a* equal to 5.68 Å) and confirmed the presence of another pyrite-type compound (IrS_3) in the Ir–S system. It

has been recently shown, however, that the IrS_2 phase is orthorhombic (*Pnam*), with the structural formula $Ir^{3+}S^{2-}(S_2)^{2-}{}_{1/2}$ (Jobic *et al.* 1990). In the absence of reports to the contrary, IrS_3 is the only S-rich pyrite-type phase, reported also as $IrS_{2.7}$ with *a* equal to 5.59 Å (Colell *et al.* 1994, and reference therein). Alternatively, the formulae of the reported phases $IrS_{2.7}$ and IrS_3 could be presented as $Ir_{0.74}S_2$ and $Ir_{0.67}S_2$, respectively, consistent with the generalized formula $Ir_{1-x}S_2$, which assumes vacancies in metal sites. This latter model is

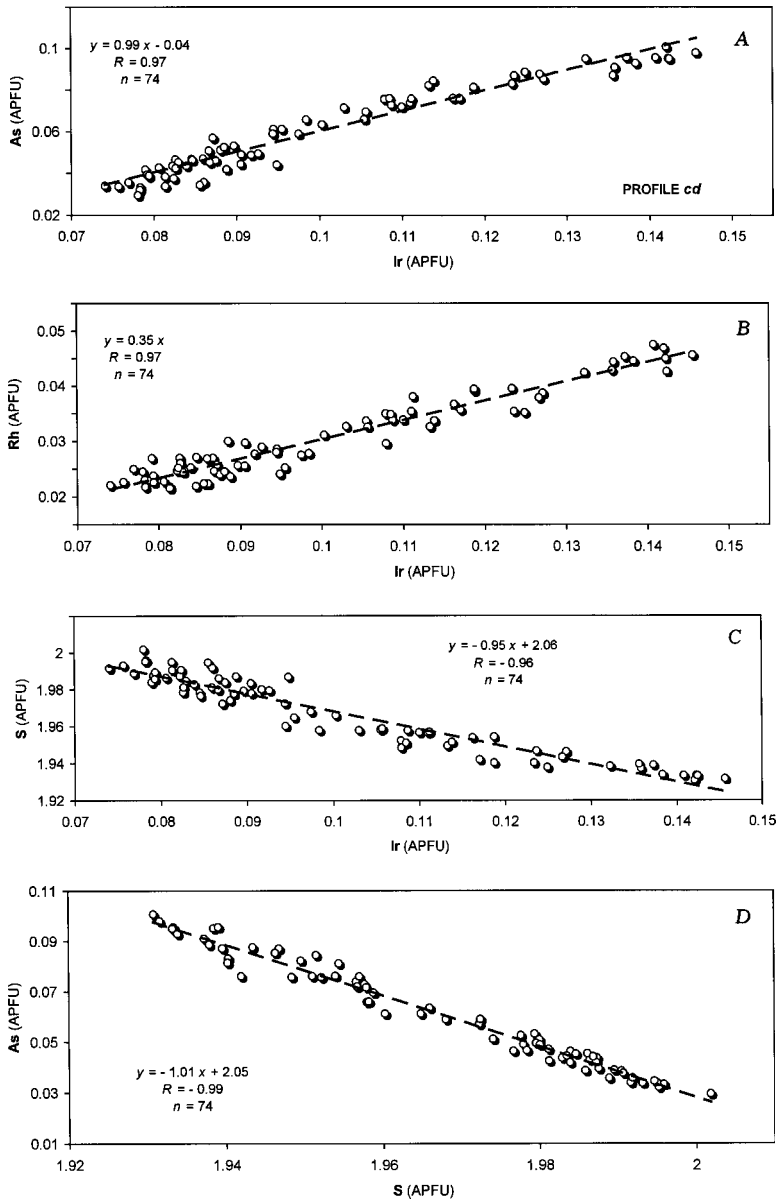

FIG. 8. Correlations of Ir and As (A), Ir and Rh (B), Ir and S (C), and S and As (D) (in *apfu*; Σatoms = 3) in compositions of the zoned laurite – erlichmanite from the Penikat complex. Results of seventy-four WDS analyses, which refer to the profile *cd*, are plotted; the location of this profile is shown in Figure 2A.

TABLE 5. COMPOSITIONS OF ZONED LAURITE–ERLICHMANITE AND IRARSITE–HOLLINGWORTHITE (PROFILE *ef*), PENIKAT LAYERED COMPLEX, FINLAND

	Ru	Os	Ir	Rh	Pd	Fe	Ni	As	S	Total
1	2.78	0.52	47.85	9.17	n.d.	0.05	0.09	23.80	14.72	98.98
2	2.84	0.65	48.49	9.06	n.d.	0.03	0.06	23.48	14.68	99.29
3	2.96	0.50	49.01	8.76	n.d.	0.03	0.05	23.35	14.76	99.42
4	2.83	0.46	49.63	7.89	0.03	n.d.	0.06	23.37	14.62	98.89
5	2.98	0.51	49.36	7.73	0.01	0.01	0.05	23.04	14.70	98.39
6	3.13	0.45	50.47	7.28	0.05	n.d.	0.07	23.01	14.57	99.03
7	2.95	0.49	50.98	6.89	n.d.	n.d.	0.04	22.99	14.48	98.82
8	37.11	7.18	15.28	2.05	0.07	0.62	0.14	3.93	32.96	99.34
9	34.61	8.24	16.85	2.23	n.d.	0.68	0.14	4.28	32.21	99.24
10	36.60	8.46	14.34	1.89	0.01	0.70	0.15	3.09	33.56	98.80
11	38.84	10.26	11.42	1.58	n.d.	0.61	0.13	1.95	34.54	99.33
12	38.35	11.09	11.21	1.43	n.d.	0.57	0.09	1.83	34.39	98.96
13	38.14	11.67	10.93	1.51	0.04	0.58	0.12	1.87	34.50	99.36
14	37.23	11.40	11.39	1.49	0.03	0.62	0.10	2.08	33.92	98.26
15	36.89	11.08	12.53	1.66	0.03	0.44	0.11	2.55	33.56	98.85
16	37.11	10.19	13.01	1.84	0.03	0.46	0.10	2.80	33.28	98.82
17	38.09	8.67	13.36	1.82	n.d.	0.46	0.09	2.97	33.33	98.79
18	39.58	7.43	12.66	1.76	0.03	0.50	0.09	2.65	34.09	98.79
19	38.15	12.04	10.67	1.52	n.d.	0.52	0.10	1.53	34.23	98.76
20	37.81	13.03	10.42	1.36	0.03	0.50	0.09	1.61	34.16	99.01
21	37.46	13.36	10.68	1.46	n.d.	0.50	0.08	1.54	33.86	98.94
22	36.91	13.53	10.89	1.44	n.d.	0.50	0.10	1.64	33.93	98.94
23	35.68	14.76	10.88	1.47	0.21	0.67	0.10	1.48	33.83	99.08
24	35.38	14.53	11.09	1.50	n.d.	0.68	0.10	1.58	33.63	98.49
25	35.05	14.64	11.35	1.54	0.09	0.68	0.14	1.70	33.55	98.74
26	35.29	14.36	11.47	1.62	0.05	0.47	0.08	1.82	33.55	98.71
27	35.71	14.35	11.28	1.59	0.02	0.49	0.08	1.85	33.22	98.59
28	35.49	14.65	11.22	1.54	n.d.	0.49	0.08	1.67	33.73	98.87
29	36.69	13.43	10.96	1.63	n.d.	0.50	0.11	1.63	33.50	98.45
30	36.53	13.63	11.02	1.58	0.11	0.50	0.09	1.66	34.11	99.23
31	37.14	13.19	10.80	1.60	n.d.	0.49	0.09	1.52	33.83	98.66
32	37.63	12.86	10.49	1.45	0.01	0.50	0.07	1.51	34.10	98.62
33	37.48	12.74	10.56	1.22	0.01	0.54	0.07	1.37	34.26	98.25
34	39.30	8.31	12.77	1.60	n.d.	0.61	0.13	2.03	33.91	98.66
35	36.80	8.69	14.53	2.13	n.d.	0.53	0.12	3.03	32.98	98.81
36	36.58	10.68	12.96	1.78	0.18	0.69	0.12	2.39	33.67	99.05
37	38.12	10.90	11.97	1.67	0.10	0.62	0.12	2.05	34.31	99.86
38	40.18	10.09	10.51	1.57	0.02	0.60	0.10	1.55	34.92	99.54
39	41.77	8.24	10.38	1.38	0.04	0.61	0.11	1.60	35.04	99.17
40	3.33	0.75	49.42	7.73	n.d.	0.02	0.03	22.85	14.65	98.78
41	3.13	0.59	49.47	8.31	n.d.	0.02	0.03	23.32	14.70	99.57
42	3.29	0.80	48.54	8.78	n.d.	0.05	0.07	23.33	15.02	99.88
43	2.93	0.69	47.59	9.23	0.09	0.06	0.05	23.36	14.47	98.47
44	3.01	0.65	47.92	9.62	n.d.	0.07	0.05	23.42	14.48	99.22

The results of these WDS analyses, from 1 to 44, are representative of the profile *ef* (Fig. 3A); they are listed (in wt.%) in order from the point *e* to the point *f*. Numbers 1–7 and 40–44: irarsite–hollingworthite. Numbers 8–39: laurite–erlichmanite. Results of the entire set of analyses obtained in the profile *ef* are presented in Figures 9A to10B.

TABLE 6. ATOM PROPORTIONS OF ZONED LAURITE–ERLICHMANITE AND IRARSITE–HOLLINGWORTHITE (PROFILE *ef*), PENIKAT COMPLEX, FINLAND

	Ru	Os	Ir	Rh	Pd	Fe	Ni	*Me*	As	S	As+S
1	0.07	0.007	0.65	0.233	-	0.002	0.004	0.97	0.83	1.20	2.03
2	0.07	0.009	0.66	0.231	-	0.002	0.003	0.98	0.82	1.20	2.02
3	0.08	0.007	0.67	0.223	-	0.001	0.002	0.98	0.82	1.21	2.03
4	0.07	0.006	0.68	0.203	<0.001	-	0.003	0.97	0.82	1.21	2.03
5	0.08	0.007	0.68	0.199	<0.001	<0.001	0.002	0.97	0.82	1.22	2.04
6	0.08	0.006	0.70	0.188	0.001	-	0.003	0.98	0.82	1.21	2.03
7	0.08	0.007	0.71	0.179	-	-	0.002	0.97	0.82	1.21	2.03
8	0.69	0.071	0.15	0.037	0.001	0.021	0.004	0.97	0.10	1.93	2.03
9	0.65	0.083	0.17	0.041	-	0.023	0.005	0.97	0.11	1.92	2.03
10	0.68	0.083	0.14	0.034	<0.001	0.024	0.005	0.96	0.08	1.96	2.04
11	0.71	0.099	0.11	0.028	-	0.020	0.004	0.97	0.05	1.98	2.03
12	0.70	0.108	0.11	0.026	-	0.019	0.003	0.97	0.05	1.99	2.04
13	0.70	0.113	0.11	0.027	<0.001	0.019	0.004	0.97	0.05	1.99	2.04
14	0.69	0.112	0.11	0.027	<0.001	0.021	0.003	0.97	0.05	1.98	2.03
15	0.69	0.110	0.12	0.030	<0.001	0.015	0.004	0.97	0.06	1.97	2.03
16	0.69	0.101	0.13	0.034	<0.001	0.015	0.003	0.97	0.07	1.96	2.03
17	0.71	0.086	0.13	0.033	-	0.015	0.003	0.97	0.07	1.95	2.02
18	0.72	0.072	0.12	0.032	<0.001	0.017	0.003	0.97	0.07	1.97	2.04
19	0.70	0.118	0.10	0.027	-	0.017	0.003	0.97	0.04	1.99	2.03
20	0.70	0.128	0.10	0.025	<0.001	0.017	0.003	0.97	0.04	1.99	2.03
21	0.70	0.132	0.10	0.027	-	0.017	0.003	0.98	0.04	1.98	2.02
22	0.69	0.134	0.11	0.026	-	0.017	0.003	0.97	0.04	1.99	2.03
23	0.67	0.146	0.11	0.027	0.004	0.022	0.003	0.97	0.04	1.99	2.03
24	0.66	0.145	0.11	0.028	-	0.023	0.003	0.97	0.04	1.99	2.03
25	0.66	0.146	0.11	0.028	0.002	0.023	0.004	0.97	0.04	1.98	2.02
26	0.66	0.143	0.11	0.030	0.001	0.016	0.002	0.97	0.05	1.99	2.04
27	0.67	0.144	0.11	0.029	<0.001	0.017	0.003	0.98	0.05	1.97	2.02
28	0.66	0.146	0.11	0.028	-	0.016	0.002	0.97	0.04	1.99	2.03
29	0.69	0.134	0.11	0.030	-	0.017	0.003	0.98	0.04	1.98	2.02
30	0.68	0.134	0.11	0.029	0.002	0.017	0.003	0.97	0.04	1.99	2.03
31	0.69	0.130	0.11	0.029	-	0.017	0.003	0.98	0.04	1.99	2.03
32	0.70	0.127	0.10	0.026	<0.001	0.017	0.002	0.97	0.04	1.99	2.03
33	0.69	0.125	0.10	0.022	<0.001	0.018	0.002	0.97	0.03	2.00	2.03
34	0.72	0.081	0.12	0.029	-	0.020	0.004	0.98	0.05	1.97	2.02
35	0.69	0.086	0.14	0.039	-	0.018	0.004	0.98	0.08	1.94	2.02
36	0.68	0.105	0.13	0.032	0.003	0.023	0.004	0.97	0.06	1.97	2.03
37	0.70	0.106	0.12	0.030	0.002	0.021	0.004	0.97	0.05	1.98	2.03
38	0.73	0.097	0.10	0.028	<0.001	0.020	0.003	0.97	0.04	1.99	2.03
39	0.75	0.079	0.10	0.024	<0.001	0.020	0.003	0.98	0.04	1.99	2.03
40	0.09	0.010	0.68	0.199	-	<0.001	0.001	0.98	0.81	1.21	2.02
41	0.08	0.008	0.68	0.212	-	0.001	0.001	0.98	0.82	1.20	2.02
42	0.08	0.011	0.66	0.221	-	0.002	0.003	0.98	0.81	1.22	2.03
43	0.08	0.010	0.65	0.237	0.002	0.003	0.002	0.98	0.82	1.19	2.01
44	0.08	0.009	0.65	0.245	-	0.003	0.002	0.99	0.82	1.19	2.01

The analytical results (in wt.%) are listed in Table 5 (profile *ef*: Fig. 3A). Numbers 1–7 and 40–44: irarsite–hollingworthite. Numbers 8–39: laurite–erlichmanite. The atom proportions are based on three atoms per formula unit.

corroborated by the disordered distribution of Rh and the presence of vacancies in the pyrite-type phase $Rh_{1-x}Se_2$, with $0.02 \le x \le 0.24$ (Kjekshus *et al.* 1979).

Thus, we suggest that Ir could be incorporated in As-free Lrt–Erl according to the following scheme of substitution: $[0.667\ Ir^{3+} + 0.333\ ^{Me}\square = (Ru + Os)^{2+}]$, which assumes that all Ir occurs as 3+ in $Ir_{0.67}S_2$ (*i.e.*, ideal "IrS_3"). In the case of the other reported S-rich phase ($IrS_{2.7}$), the formula $Ir_{0.74}S_2$ indicates an "excessive" Ir charge, which is inconsistent with the formal 3+ valence for Ir and implies a mixed-valence character for this phase. If the solid solution extends toward $Ir_{0.74}S_2$, the following scheme of substitution is suggested to incorporate Ir in Lrt–Erl: $[0.52\ Ir^{3+} + 0.22\ Ir^{2+} + 0.26\ ^{Me}\square = (Ru + Os)^{2+}]$. The partial reduction of Ir to 2+ is consistent with the presence of Ir^{2+} in a newly reported pyrite-type $Ir^{2+}(Te_2)^{2-}$ ditelluride (Jobic *et al.* 2001).

The existence of limited solid-solutions extending from $(Ru,Os)S_2$ toward the pyrite-type $Ir_{1-x}S_2$ ("IrS_3") is confirmed by the synthesis of mixed single crystals of the type $Ir_{0.667+x}Ru_{1-x}S_2$, with $0 < x < 1$ (Colell *et al.* 1994). The synthetic $Ir_xRu_{1-x}S_2$ phases ($0.005 < x < 0.5$) have a pyrite structure, but the presence of small amounts of orthorhombic IrS_2 (*cf.* Jobic *et al.* 1990) was observed in the X-ray-diffraction patterns at higher content of Ir (Colell *et al.* 1994).

The limited nature of the $Ir_x(Ru,Os)_{1-x}S_2$ solid solutions is well recognized in natural samples. A complete and continuous series of solid solution has been established between the RuS_2 and OsS_2 end-members (Lrt–Erl series), whereas the content of "IrS_2" is less than 20 mol.% in these samples worldwide (*e.g.*, Cabri *et al.* 1996). We suggest that this limit is a result of the existence of vacancy-type defects, and related complications thus arise from the incorporation of Ir by substitution schemes of the type $[0.667\ Ir^{3+} + 0.333\ ^{Me}\square = (Ru + Os)^{2+}]$ or $[0.52\ Ir^{3+} + 0.22\ Ir^{2+} + 0.26\ ^{Me}\square = (Ru + Os)^{2+}]$. Thus a suggestion on the existence of "complete solid solution among RuS_2–OsS_2–IrS_2", made by Jen & Teng (1973) [cited in Craig & Scott 1974], is unlikely to be correct.

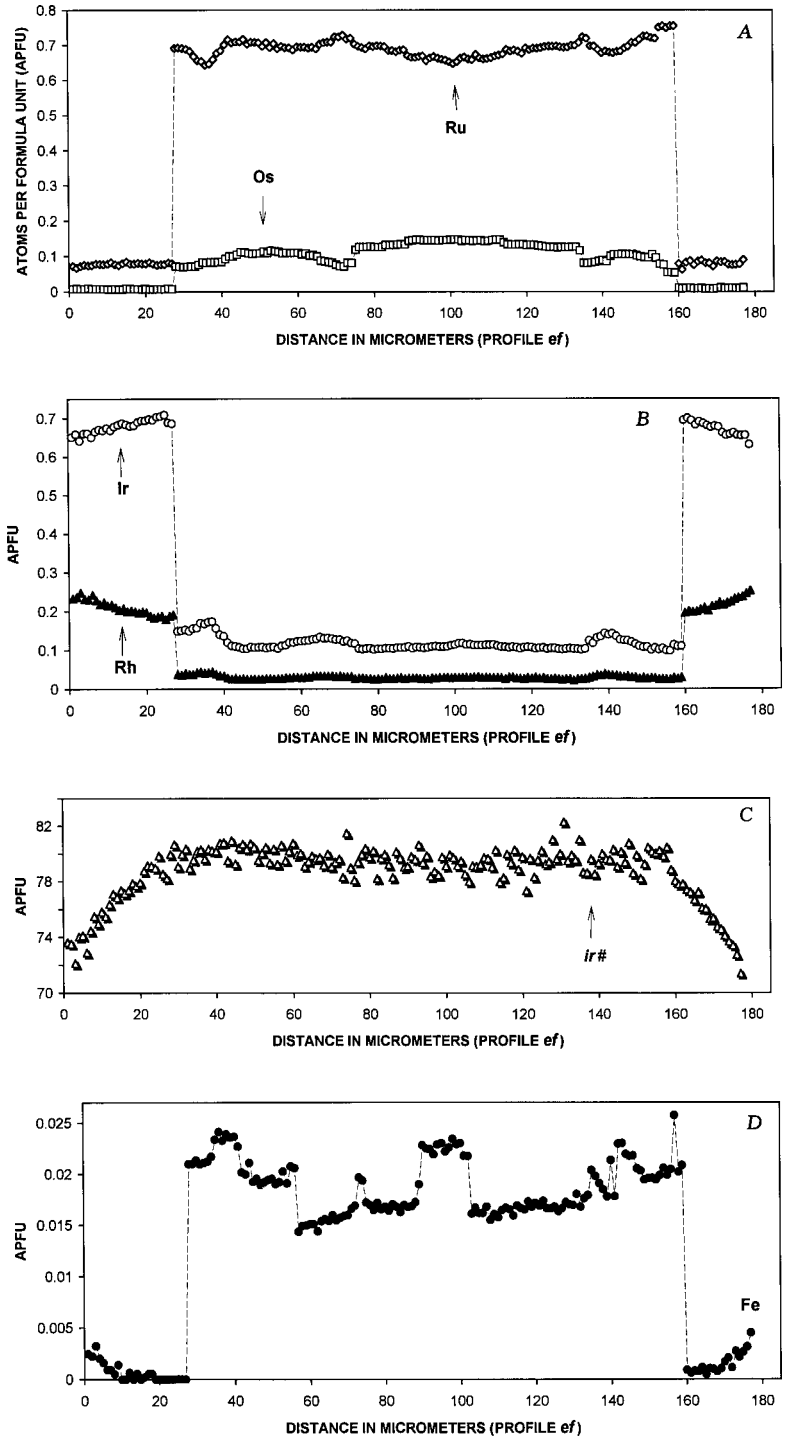
A
ATOMS PER FORMULA UNIT (APFU)
Ru
Os
DISTANCE IN MICROMETERS (PROFILE ef)
B
APFU
Ir
Rh
DISTANCE IN MICROMETERS (PROFILE ef)
C
APFU
ir#
DISTANCE IN MICROMETERS (PROFILE ef)
D
APFU
Fe
DISTANCE IN MICROMETERS (PROFILE ef)

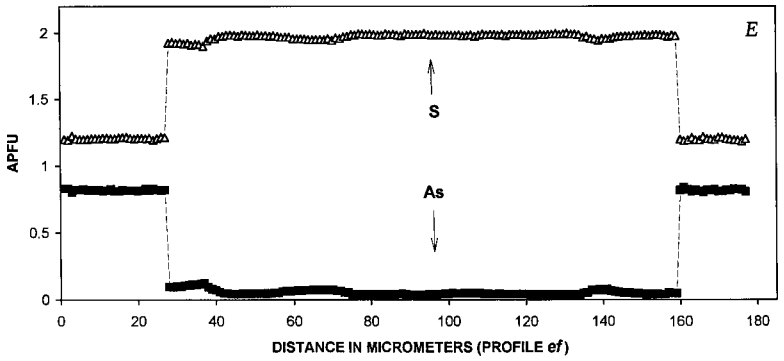

FIG. 9. Variations in concentrations of Ru, Os (A), Rh, Ir (B), Fe (D), S and As (E), and values of the *ir*# index [*i.e.*, 100 Ir / (Ir + Rh)] (C), expressed in *apfu*: Σatoms = 3, along electron-microprobe profile *ef* across the zoned grain shown in Figure 3A.

TABLE 7. COMPOSITION OF LAURITE–ERLICHMANITE FROM THE PENIKAT COMPLEX, FINLAND

	Ru	Os	Ir	Rh	Pt	Pd	Fe	Ni	As	S	Total
1	37.23	22.51	4.26	0.88	n.d.	0.07	0.14	0.06	n.d.	33.89	99.04
2	32.63	26.95	5.60	0.66	n.d.	n.d.	0.13	0.05	n.d.	33.08	99.10
3	31.95	27.25	5.75	0.77	n.d.	0.05	0.13	0.04	n.d.	33.08	99.02
4	32.94	26.77	5.09	0.62	0.03	n.d.	0.15	0.05	n.d.	33.43	99.08

	Ru	Os	Ir	Rh	Pt	Pd	Fe	Ni	*Me*	As	S
1	0.70	0.22	0.04	0.02	-	0.001	0.005	0.002	0.99	-	2.01
2	0.63	0.28	0.06	0.01	-	-	0.004	0.002	0.98	-	2.02
3	0.62	0.28	0.06	0.01	-	0.001	0.005	0.001	0.98	-	2.02
4	0.63	0.27	0.05	0.01	<0.001	-	0.005	0.002	0.98	-	2.02

Numbers 1 to 4 refer to different parts of the laurite–erlichmanite grain shown in Figure 4A. Compositions are first reported in wt.%. Below, the atom proportions are reported, calculated on the basis of three atoms per formula unit (*apfu*).

The incorporation of Rh in laurite – erlichmanite

Pure RhS_2 does not exist in the Rh–S system (Hulliger 1964), and the powder-diffraction pattern of the "Rh_2S_5" phase, synthesized by reaction of $RhCl_3$ with S at 600°C (Wöhler *et al.* 1933), is similar to that of pyrite (Juza *et al.* 1935). This phase has been also reported as "RhS_3", with a pyrite-type structure and *a* equal to 5.58 Å (Berlincourt *et al.* 1981). Makovicky *et al.* (2002) reported that in the system Fe–Rh–S at 900° and 500°C, the RhS_3 pyrite phase has the composition "$Rh_{2.75}S_{7.25}$", which corresponds to a Rh:S ratio (0.38), closer to Rh_2S_5 (0.40) than to RhS_3 (0.33). Barkov & Fleet (2004) reported the occurrence of a natural phase $(Pt_{0.78}Rh_{0.20}Ir_{0.03})_{\Sigma 1.01}(As_{1.53}S_{0.47})_{\Sigma 2.00}$, with a Rh:S ratio of 0.43, which represents a solid solution from $PtAs_2$ toward the pyrite-type $Rh_{1-x}S_2$ (*i.e.*, toward "Rh_2S_5" rather than toward "RhS_3").

Formulae of the pyrite-type phase of Rh may be represented as $Rh_{0.667}S_2$ (*i.e.*, ideal "RhS_3") and $Rh_{0.8}S_2$ (*i.e.*, "Rh_2S_5" and "$Rh_{2.75}S_{7.25}$"). Consequently, the following two schemes, assuming the presence of vacancies, may be suggested for the incorporation of Rh in Lrt–Erl: (1) [0.667 Rh^{3+} + 0.333 $^{Me}\square$ = $(Ru + Os)^{2+}$], and (2) [0.4 Rh^{3+} + 0.4 Rh^{2+} + 0.2 $^{Me}\square$ = $(Ru + Os)^{2+}$]. Scheme 2 suggests the mixed-valence character of the pyrite-type $Rh_{1-x}S_2$ phase, *i.e.*, $Rh^{3+}{}_{0.4}Rh^{2+}{}_{0.4}S_2$ with a ratio Rh^{2+}: Rh^{3+} of 1:1, consistent with a ratio Rh:Co of 1:1, observed in synthetic $Co_{0.5}Rh_{0.5}S_2$ crystallizing in the pyrite structure with *a* equal to 5.639 Å (Hulliger 1964).

The behavior and incorporation of Fe in laurite – erlichmanite

Our data indicate that substantial levels of Fe are present in Lrt–Erl of this study (Tables 1–5); note that contamination (*i.e.*, fluorescence from an Fe-rich phase) can be ruled out, because the Lrt–Erl grains are enclosed by epoxy (Figs. 2A, 3A). Also, we observed that Fe is preferentially incorporated in Lrt–Erl relative to the associated Irs–Hlw (Figs. 5C, 7D, 9D).

The only reported occurrence of a natural $Fe_xRu_{1-x}S_2$ solid solution is that from the Imandra layered complex, Kola Peninsula, Russia [$(Fe_{0.81}Ru_{0.14}Os_{0.007}Ir_{0.004})_{\Sigma 0.96}S_{2.04}$: Barkov & Fleet 2004]. Special conditions are presumably required to stabilize this solid solution. Tsay *et al.* (1994) experienced difficulties in their attempts to synthesize samples of $Fe_xRu_{1-x}S_2$ solid solution; they found that only minor Fe substitutes for Ru, and noted that the distribution of Fe is inhomogeneous. However, phases of the type $Fe_xRu_{1-x}S_2$, with x = 0.1, 0.2, 0.3, 0.5, 0.9, have been synthesized by Hwang *et al.* (1994) using oscillating chemical vapor transport. Synthetic RuS_2 doped with FeS_2, $FeAs_2$ and Fe has been characterized by Schuler & Siebert (1995) and Schuler *et al.* (1995). Karup-Møller & Makovicky (2002) observed that the solubility of Fe in synthetic OsS_2 (erlichmanite) increases with increasing sulfur fugacity

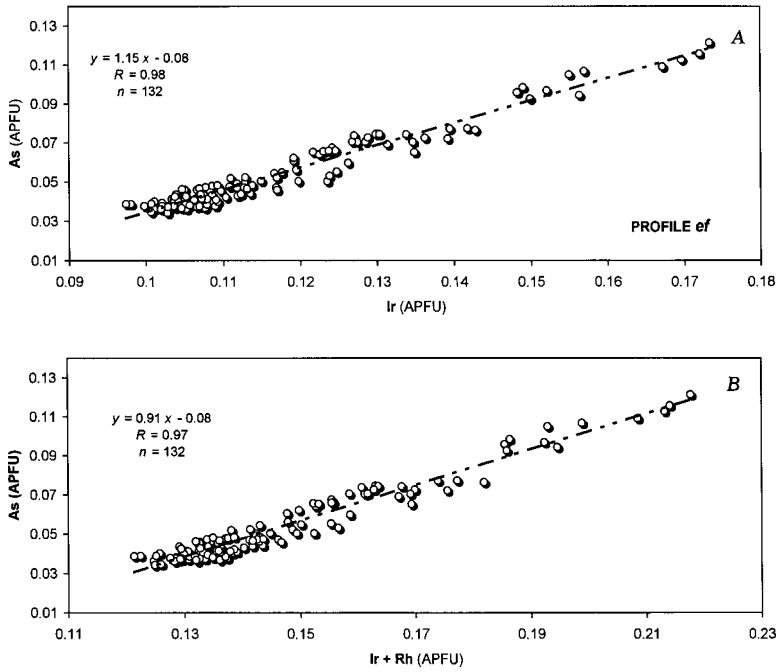

FIG. 10. Correlations of Ir and As (A) and (Ir + Rh) and As (B) (in *apfu*: Σatoms = 3) in compositions of the zoned laurite–erlichmanite from the Penikat complex. Results of 132 WDS analyses, which refer to the profile *ef*, are plotted; the location of this profile is shown in Figure 3A.

$f(S_2)$ and decreasing temperature (0.2–1.1 at.% Fe at 1180°C, and up to 5.7 at.% Fe at 900°C).

Tsay *et al.* (1994) reported that minor Fe occurs in its "normal" ferrous valence state (2+) in synthetic RuS_2. However, Schuler *et al.* (1997) studied synthetic RuS_2 doped with Fe^{3+} and suggested that a compensation mechanism takes place, in which the incorporated Fe^{3+} accepts one electron and converts to Fe^{2+}. It is known that compensation effects commonly result in an inhomogeneous distribution of impurities. The distribution of Fe is indeed quite heterogeneous in the zoned Lrt–Erl grains (Figs. 7D, 9D); this feature is consistent with a compensation mechanism. In addition, the valence of the incorporated Fe (3+) could well be a reflection of the oxidizing character of the environment at Kirakkajuppura, which is evident from the presence of abundant Pd–Pb oxide ($Pd^{2+}{}_7Pb^{2+}O_8$ or $Pd^{2+}{}_9Pb^{2+}O_{10}$: Barkov *et al.* 1999a). Also, the incorporation of Fe^{3+} in the Lrt–Erl is consistent with synthesis of the pyrite-like $Fe^{3+}S^{2-}(S_2)^{2-}{}_{1/2}$ phase, which contains Fe^{3+} and is "intermediate" between the layered chalcogenides $[Me^{4+}(S^{2-})_2]$ and the pyrite-type compounds $[Me^{2+}(S_2)^{2-}]$ (Brec *et al.* 1989). On the other hand, Fe content, in general, clearly increases toward the margin in the zoned grains (Figs. 7D, 9D), and a normal decrease in temperature during the crystallization could be thus crucial to control the observed distribution and behavior of Fe. Variations in $f(S_2)$ could in general be of less importance, as is indicated by the antipathetic behavior of Fe and Os ($R = -0.94$) in the *cd* profile of Lrt–Erl (Figs. 7A, D). However, there is an abrupt increase in Fe in the center of the Lrt–Erl grain of Figure 9D, in the zone with the maximum content of Os (*i.e.*, "white" zone in the center of the "red" crystal: Fig. 3B); thus, the Fe enrichment in this zone could reflect a higher level of $f(S_2)$ during crystallization.

Results of the *cd* profile reveal the following correlations: Fe *versus* Ru ($R = 0.91$), Fe *versus* As ($R = -0.54$), and Fe *versus* S ($R = 0.56$: $n = 74$), which imply a substitution of the type $(Fe + Ru)^{2+} = Os^{2+}$, probably coupled with a minor S-for-As substitution. The Fe-for-Ru substitution seems relevant in the Fe–Os-enriched zone in the Lrt–Erl (Fig. 9D), whereas Fe may substitute for both Os and Ru in the other zones of this grain.

In contrast, Fe is intimately associated with As in the other grain of Lrt–Erl (Figs. 1A, 5A–C), where structural factors appear to have exerted a major control over the distribution of Fe, consistent with a solid solution toward $Me(S,As)_2$ in the approximate ratio (Ir + Rh + Fe):As of 2.5:1.

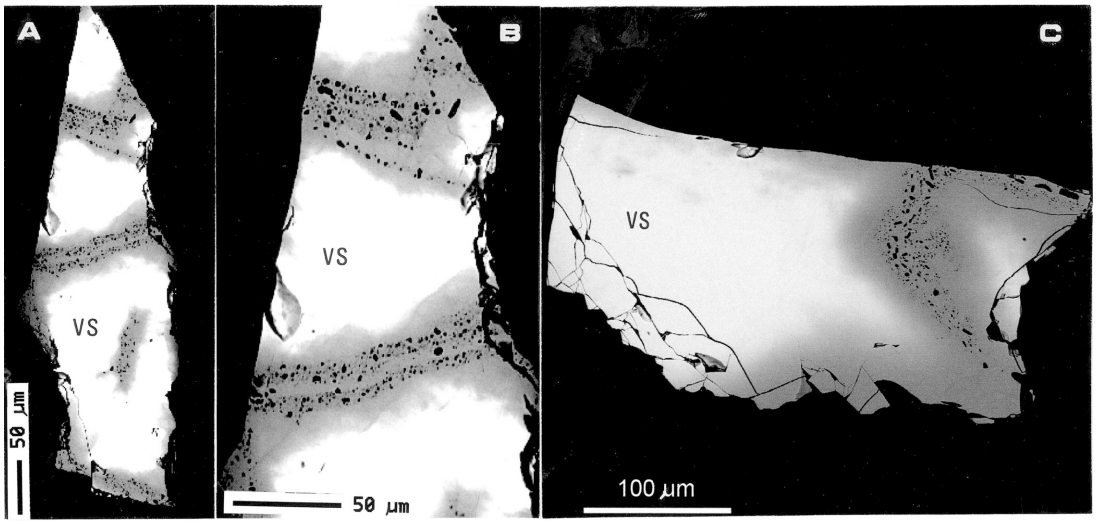

FIG. 11. A–C. Examples of compositional zoning in large grains of vysotskite–braggite (VS) from the Penikat complex. Note the close association of the alteration zones (gray) with abundant micro-inclusions of a hydrous silicate(s) (black). B. Magnification of upper part of the grain shown in A. Note that submicrometric grains of a hydrous silicate(s) form separate bands in the altered vysotskite – braggite. BSE images; the surrounding material is epoxy.

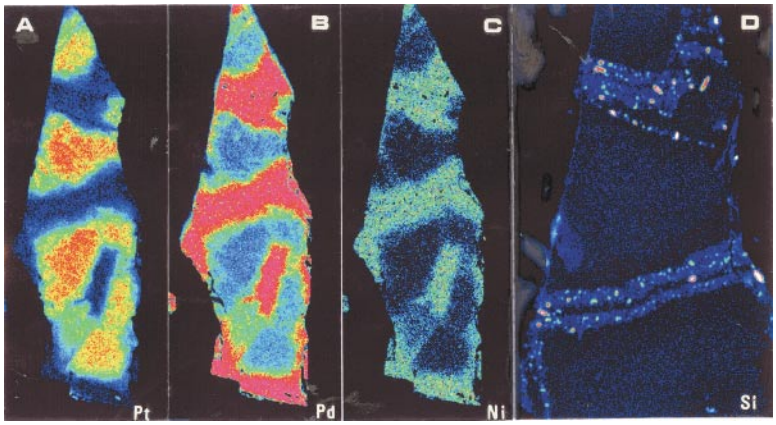

FIG. 12. X-ray maps showing the distribution of Pt (A), Pd (B) and Ni (C) in the zoned grains of vysotskite – braggite (Fig. 11). The change in color is indicative of compositional variations: red is the highest concentration, followed by orange, yellow, green, blue, dark blue, and violet. The silicon X-ray map shown in D illustrates the bands of submicrometric hydrous silicate(s), which are intimately associated with the alteration zones in the vysotskite – braggite (Fig. 11B).

The incorporation of Ru and Fe in irarsite – hollingworthite

The content of Ru (+Os) in the zoned Irs–Hlw is approximately 0.1 *apfu*, and is accompanied by a relative deficit in As and corresponding excess in S (*ca.* 0.2 *apfu*: Tables 3–6, Figs. 7A, E, 9A, E), thus indicating the incorporation of Ru in the form of the laurite component *via* the following charge-balance substitution: $[Ru^{2+} + (S_2)^{2-} = Me^{3+} + (AsS)^{3-}]$. The amount of ruthe-

nium correlates negatively with that of Rh and, in contrast, slightly positively with that of Ir; thus, the incorporation of Ru in the Irs–Hlw is likely dominated by the Ru-for-Rh substitution. This scheme is consistent with the negative S–As correlation (R = –0.79 and –0.71: Fig 7E, 9E). Evidence for this scheme in the hollingworthite – laurite – erlichmanite series was also reported from the Coldwell complex, Ontario, Canada (Ohnenstetter *et al.* 1991). However, Ir is dominant over Rh in the compositions of members of the Irs–Hlw series from the Penikat complex (Figs. 7B, 9B, Tables 3–6), whereas the sulfarsenides from the Coldwell complex are, in contrast, rich in Rh and very poor in Ir.

The following correlations are also observed in the zoned Irs–Hlw (profiles *cd* and *ef*, respectively): Ir *versus* Rh (R = –0.98 and –0.96), Ir *versus* Fe (R = –0.82 each), and Rh *versus* Fe (R = 0.75 and 0.83). They indicate that the incorporation of Fe in the Irs–Hlw is governed by the following mechanism of substitution: $(Rh + Fe)^{3+} = Ir^{3+}$; Fe likely occurs as the arsenopyrite component $[Fe^{3+}(AsS)^{3-}]$ in the zoned Irs–Hlw.

The presence of other elements in laurite – erlichmanite

The possible presence of Cr (up to 0.8 wt.%) was reported in Lrt–Erl from the Baula complex, India (Augé *et al.* 2002); also, these authors cited other occurrences of "Cr-bearing Lrt–Erl" from the Bushveld complex. This report stimulated us to check for Cr in samples of Lrt–Erl from the Penikat complex; Cr was carefully sought, but was not detected in various zones of the five large grains (Figs. 1 to 4). Sulfides bearing Cr, Ti and V are extremely rare; for example, pyrrhotite is one of the most common BMS, but there is so far only a single reported occurrence of terrestrial pyrrhotite containing Ti (Barkov *et al.* 2000). Theoretically, minor Cr could enter $(Ru,Os)S_2$ (*e.g.*, Schuler & Siebert 1995). However, Cr has a strong lithophile character, and the incorporation of Cr in a sulfide would require the existence of a highly reducing environment, which is not indicated by minerals in association with the Lrt–Erl in the Baula complex. A more detailed characterization of the "Cr-bearing Lrt–Erl" is required to exclude possible interference from an underlying mineral(s) enriched in Cr, which commonly occur in association with Lrt–Erl.

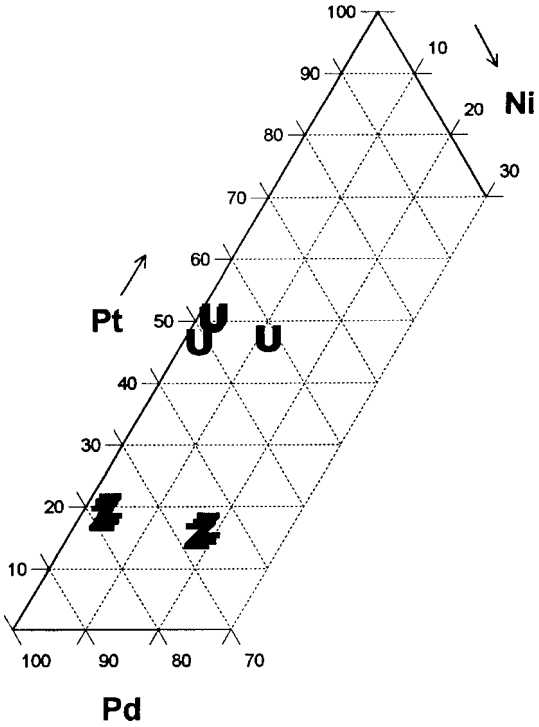

FIG. 13. Compositions of zoned vysotskite – braggite from the Penikat complex in the Pd–Pt–Ni compositional space (atom %). Symbols: U: unaltered vysotskite – braggite, Z: zones of alteration (Figs. 11A–C, Table 8).

TABLE 8. COMPOSITIONS OF ZONED VYSOTSKITE–BRAGGITE FROM THE PENIKAT LAYERED COMPLEX, FINLAND

wt.%	Pt	Pd	Ni	Fe	S	Total
1	51.03	30.75	0.66	0.02	18.80	101.26
2	25.63	52.39	1.26	0.01	21.47	100.76
3	54.00	27.06	0.61	n.d.	18.54	100.21
4	24.87	52.36	1.27	n.d.	21.53	100.03
5	23.91	53.76	1.27	0.02	21.55	100.51
6	54.23	27.26	0.61	n.d.	18.62	100.72
7	23.24	54.29	1.34	0.02	21.72	100.61
8	52.61	24.93	3.77	n.d.	19.08	100.39
9	52.75	24.82	3.85	n.d.	19.39	100.81
10	22.79	47.89	7.27	n.d.	22.66	100.61
11	21.28	47.68	7.22	0.08	22.63	98.89
12	20.05	48.24	7.11	0.02	23.07	98.49
13	41.86	38.46	0.34	n.d.	19.28	99.94
14	44.22	36.13	0.40	n.d.	18.86	99.61

apfu	Pt	Pd	Ni	Fe	*Me*	S
1	0.46	0.50	0.02	<0.001	0.98	1.02
2	0.20	0.75	0.03	<0.001	0.98	1.02
3	0.49	0.45	0.02	-	0.97	1.03
4	0.19	0.75	0.03	-	0.98	1.02
5	0.19	0.76	0.03	<0.001	0.98	1.02
6	0.49	0.46	0.02	-	0.97	1.03
7	0.18	0.77	0.03	<0.001	0.98	1.02
8	0.46	0.40	0.11	-	0.98	1.02
9	0.46	0.40	0.11	-	0.97	1.03
10	0.17	0.64	0.18	-	0.99	1.01
11	0.16	0.65	0.18	0.002	0.98	1.02
12	0.15	0.65	0.17	<0.001	0.97	1.03
13	0.36	0.61	0.01	-	0.98	1.02
14	0.39	0.58	0.01	-	0.99	1.01

Numbers 1 to 7 refer to the vysotskite–braggite grain shown in Figures 11A, B. Analyses 1, 3 and 6: different areas of the unaltered grain (*i.e.*, "white" phase: Figs. 11A, B). Analyses 2, 4 and 7: zones of alteration in this grain (*i.e.*, "gray" phase: Figs. 11A, B). Numbers 8 to 12 refer to the vysotskite–braggite grain shown in Figure 11C. Analyses 8 and 9: different areas of the unaltered grain (*i.e.*, "white" phase: Fig. 11C). Analyses 10, 11 and 12: zones of alteration in this grain (*i.e.*, "gray" phase: Fig. 11C). Numbers 13 and 14 refer to vysotskite–braggite, which is the host of the zoned grain of laurite–erlichmanite shown in Figure 1A. The atom proportions are based on two atoms per formula unit (*apfu*).

The samples of Lrt–Erl examined from the Penikat complex are very poor in Ni (Tables 1 to 5). Nevertheless, natural occurrences of nickeloan Lrt–Erl can be reasonably expected, consistent with the experimental data (Zviadadze *et al.* 1981, De Los Reyes *et al.* 1993). It is known that the NiS–NiS_2 buffer curve is located above the Os–OsS_2 and Ru–RuS_2 buffers; thus, an elevated level of $f(S_2)$ would have promoted the solid solution of Lrt–Erl toward vaesite, the pyrite-type NiS_2. Also, re-equilibration between chromite and sulfide could have resulted in a relative increase in Ni and $f(S_2)$ in the remaining sulfide, thus promoting crystallization of members of the laurite – vaesite series in chromitite. This is consistent with the occurrence of ruthenoan pyrite in a chromitite layer (Barkov & Fleet 2004). Also, the existence of the laurite – cattierite (CoS_2) solid solution may be expected.

Other possible examples of solid solutions among pyrite-type disulfides and cobaltite-type sulfarsenides

The compositions of some PGE sulfarsenides reported in the literature are consistent with solid solutions of the pyrite-type disulfide(s) with the cobaltite-type sulfarsenide(s). For example, a Rh–As-bearing erlichmanite [$(Os_{0.78}Rh_{0.15}Ir_{0.02}Ru_{0.02}Pt_{0.01})_{\Sigma 0.98}(S_{1.81}As_{0.21})_{\Sigma 2.02}$] from Urals, Russia (Begizov *et al.* 1976) shows an atomic (Rh + Ir):As ratio of *ca.* 1:1, and Rh is likely incorporated as a hollingworthite component *via* a coupled substitution of the type $[(Rh + Ir)^{3+} + (AsS)^{3-} = (Ru + Os)^{2+} + (S_2)^{2-}]$. A related PGM has been reported from Aikora, Papua New Guinea ["ruarsite": $(Ru_{0.67}Rh_{0.27}Ir_{0.09})_{\Sigma 1.03}(S_{1.61}As_{0.36})_{\Sigma 1.97}$: Weiser & Bachmann 1999]. The (Rh + Ir):As ratio of this PGM is 1 : 1; it is strongly As-deficient (S-excessive) relative to *Me*AsS, and may thus be a Rh–As-rich variety of laurite, implying a solid solution toward hollingworthite – irarsite, consistent with the substitution scheme that is formulated above for the Rh–As-rich erlichmanite. Also, a sample of "platarsite" has been reported from Aikora [$(Pt_{0.48}Ir_{0.40}Rh_{0.13}Os_{0.03}Ru_{0.01})_{\Sigma 0.98}(As_{1.41}S_{0.56})_{\Sigma 1.97}$: Weiser & Bachmann 1999], displaying an essential deficit in S and corresponding excess in As relative to the ideal formula of platarsite (PtAsS: Cabri *et al.* 1977, Cabri & Laflamme 1981). We also note that the (Ir + Rh):S ratio is 1:1, and this PGM may be thus a member of the sperrylite $[Pt^{2+}(As_2)^{2-}]$ – irarsite – hollingworthite series, in which $(Ir + Rh)^{3+}$ substitutes for Pt^{2+} and $(AsS)^{3-}$ substitutes for $(As_2)^{2-}$. In addition, the charge-balance mechanism $[Rh^{3+} + (AsS)^{3-} = Pt^{4+} + (As_2)^{4-}]$ was proposed for the incorporation of Rh in the sperrylite – hollingworthite series (Barkov *et al.* 1999b). The electronic structure of $PtAs_2$ is not well understood, however, and an alternative scheme $[Rh^{3+} + (AsS)^{3-} = Pt^{2+} + (As_2)^{2-}]$, which appears more correct, has been suggested instead (Barkov & Fleet 2004). All of these examples imply that limited solid-solutions between a pyrite-type disulfide(s) (or diarsenide) and a cobaltite-type sulfarsenide(s) may be more common, and wider ranges of miscibility may exist, than it is presently recognized.

Origin of the zoning in composite grains of the PGE sulfides–sulfarsenides from the Penikat complex

The following observations have genetic implications: (1) The zoned grains exhibit a characteristic internal arrangement, with cryptic zoning and well-developed growth-related zoning, which is generally subparallel to crystal faces (Figs. 1 to 3); (2) "Evolutionary" compositional trends are observed (*e.g.*, Figs. 6A–C, 7C, 9C). (3) The alteration of early-formed zones is lacking. These characteristics imply that the zoned sulfides–sulfarsenides of the PGE crystallized as primary phases, from single microvolumes of an isolated liquid or fluid, and at conditions of a closed system. The PGE sulfarsenides, which mantle the associated Lrt–Erl (Figs. 2, 3), clearly formed after these sulfides. Probably, only limited amounts of As could be incorporated in the growing PGE sulfides at the given conditions of crystallization, thus leading to a relative increase in As to promote the deposition of the PGE sulfarsenides at a late stage. Typically, these zoned grains crystallized from the center to the margin, as is suggested, for example, by the gradual decrease in *ir*# toward the edge (Figs. 7C, 9C). This index appears to be a useful "evolutionary" indicator for the PGE-rich sulfarsenides. The gradual decrease in Ir and the corresponding decrease in Rh imply a higher temperature of crystallization of the end-member IrAsS with respect to RhAsS (*cf.* Barkov *et al.* 1999b). The maximum thermal stability of RuS_2 is very high (1275°C: Brenan & Andrews 2001), so that laurite likely crystallized at a higher temperature than irarsite, consistent with the occurrence of Irs–Hlw as the "rims" around Lrt–Erl (Figs. 2, 3). The maximum content of Ru is approximately 0.7 *apfu* in the notably zoned grains (Figs. 5A, 7A, 9A) and in the slightly zoned grains of Lrt–Erl (Figs. 4A, B, Table 7), and this consistency points to uniform conditions of crystallization in terms of levels of $f(S_2)$ and temperature. The maximum content of Ir is also *ca.* 0.7 *apfu* in various zones of the Irs–Hlw "rims" (Figs. 7B, 9B), thus implying quite uniform conditions of crystallization of these zones. Pure OsS_2 is known to crystallize at a higher $f(S_2)$ than RuS_2, and the formation of the fine-scale "rhythmic" zoning in the Lrt–Erl (*e.g.*, Figs. 2B, 3A, B) is thus best explained by the existence of rapid fluctuations in $f(S_2)$ in the environment. Thus, the Os-enriched zones (such as the Os-rich microzones shown in Fig. 3B) likely crystallized at a higher $f(S_2)$ than the associated Ru-rich zones.

Origin of the unusual "globular" microtexture observed in laurite – erlichmanite

Two alternative explanations may be suggested to account for the appearance of the unusual microglobules of zvyagintsevite and clinochlore in Lrt–Erl (Fig. 4A). (1) These globules could be interpreted as microdroplets of a complex immiscible liquid(s), containing Si, Al, Fe, Mg, H_2O (*i.e.*, clinochlore components), and Pd and Pb (zvyagintsevite components), suspended in the Ru–Os-rich sulfide liquid. They may thus have appeared upon cooling of a pre-existing single liquid, and the composite globules could have formed by the separation and gravity differentiation of the much denser Pd_3Pb. The uniformly oriented phase-boundaries observed in the two globules (shown by black arrows: Fig. 4A) are in agreement with this model. Textures of the other microglobules are not so obvious, however. This model cannot be presently tested because experimental data on such complex systems are lacking. (2) Another interpretation is that all of the main constituents of the globules (Si, Al, Fe, Mg, Pd and Pb, and H_2O) were incompatible during the crystallization of Lrt–Erl from a liquid or fluid (a hydrothermal origin of laurite appears possible: Barkov & Fleet 2004). Thus, these elements were concentrated in various H_2O-bearing "bubbles", enclosed within the Lrt–Erl. The *mg#* value of the clinochlore in a "bubble" (Fig. 4A) is 69, and this value is very close to that reported for a sample of type clinochlore associated with the PGE mineralization at Kirakkajuppura (71: Barkov *et al.* 1999a). Thus, these textural varieties of clinochlore were presumably in equilibrium with each other, and their uniform *mg#* values were likely controlled by uniform physicochemical parameters.

Origin of the zoning in vysotskite – braggite

The textures and, especially, the intimate association of the "reaction" zones of Vsk–Brg with the micro-aggregates and bands of a hydrous silicate(s) (Figs. 11A–C) suggest that these zones formed as a result of alteration of the original (unaltered) Vsk–Brg. The average contents of the PtS, PdS, and NiS end-members (in mol.%) are $[PtS_{49}PdS_{48}NiS_2]$ for the unaltered Vsk–Brg, and are $[PtS_{19}PdS_{77}NiS_3]$ for the Vsk–Brg associated with the alteration zones (Figs. 11A, B, 13, Table 7). The findings obtained for the other grain (Fig. 11C) are consistent, and the average compositions are $[PtS_{47}PdS_{41}NiS_{11}]$ for the unaltered Vsk–Brg and $[PtS_{16}PdS_{66}NiS_{18}]$ for the Vsk–Brg from the zones of alteration.

On the basis of the textural relations and compositions (Figs. 11A, B, 13, Table 7), we suggest that the original Vsk–Brg reacted with a fluid at a late stage of hydrothermal alteration. This fluid transported and introduced Pd and, to a lesser degree, Ni, and simultaneously removed Pt, which was also mobile during the alteration. Experimental data indicating that Pd-rich members of the Vsk–Brg series form at a lower temperature than the Pt-rich members (Cabri *et al.* 1978) support this suggestion; an increase in the Ni content implies a lower temperature of equilibration of the Vsk–Brg (Verryn & Merkle 2002). The Pd–(Pt) sulfides could have deposited from a hydrothermal solution at a low temperature (Tarkian *et al.* 1996). In addition, the majority of Vsk–Brg was precipitated at a late stage in the Kirakkajuppura deposit (Barkov *et al.* 1999a). Interestingly, lithophile elements also were mobile, along with Pd and Pt, in the hydrothermal fluid, and they coprecipitated with the Pd–(Ni)-rich sulfides to form the abundant micro-aggregates, bands and individual submicrometric grains associated with the late-stage Vsk–Brg in the zones of alteration (Figs. 11A–C).

Acknowledgements

Financial support from the Natural Sciences and Engineering Research Council of Canada (M.E.F., R.F.M. and A.Y.B.) and from the Academy of Finland (T.T.A.) is gratefully acknowledged. We are grateful to the staff of analytical laboratories at McGill University (Montreal), the University of Western Ontario (London, Canada), and the University of Oulu (Finland). A.Y.B. expresses his sincere thanks to Glenn Poirier (presently with CANMET, Ottawa) for his expert assistance with EMP results, to Tapio Halkoaho (Geological Survey of Finland, Kuopio, Finland) for information regarding the Penikat complex, and to the organizing committee of the IGCP Project 336 Symposium in Rovaniemi (Finland) in 1996, for its assistance in collecting samples from the Kirakkajuppura PGE deposit of the Penikat complex. We thank the referees and Associate Editor N.J. Cook for their comments on this contribution. Mr. J.H.G. Laflamme provided information concerning the respective fluorescence-yield values for Pt and Pd.

References

Alapieti, T.T. & Halkoaho, T.A.A. (1995): Cryptic variation of augite in the Penikat layered intrusion, northern Finland, with reference to megacyclic units and PGE-enriched zones. *Mineral. Petrol.* **54**, 11-24.

_____ & Lahtinen, J.J. (1986): Stratigraphy, petrology, and platinum group element mineralization of the Early Proterozoic Penikat layered intrusion, northern Finland. *Econ. Geol.* **81**, 1126-1136.

_____ & _____ (1989): Penikat Intrusion. *In* Early Proterozoic Layered Intrusions in the Northeastern Part of the Fennoscandian Shield (T. Alapieti, ed.). *Fifth Int. Platinum Symp., Guide to the Post-Symposium Field Trip, Geol. Surv. Finland, Guide* **29**, 15-21 and 209-216.

AUGÉ, T., SALPETEUR, I., BAILLY, L., MUKHERJEE, M.M. & PATRA, R.N. (2002): Magmatic and hydrothermal platinum-group minerals and base-metal sulfides in the Baula complex, India. *Can. Mineral.* **40**, 277-309.

BARKOV, A.Y. & FLEET, M.E. (2004): An unusual association of hydrothermal platinum-group minerals from the Imandra layered complex, Kola Peninsula, northwestern Russia. *Can. Mineral.* **42**, 455-467.

_____, _____, MARTIN, R.F. & HALKOAHO, T.A.A. (2004a): A potentially new konderite-like sulfide of Fe, Pb, Cu, Rh, Pd, and Ir from the Penikat layered complex, Finland. *Can. Mineral.* **42**, 499-513.

_____, _____, _____ & TARKIAN, M. (2004b): Compositional variations in oulankaite and a new series of argentoan oulankaite from the Lukkulaisvaara layered intrusion, northern Russian Karelia. *Can. Mineral.* **42**, 439-453

_____, HALKOAHO, T.A.A., ROBERTS, A.C., CRIDDLE, A.J., MARTIN, R.F. & PAPUNEN, H. (1999a): New Pd–Pb and Pb–V oxides from a bonanza-type PGE-rich, nearly BMS-free deposit in the Penikat layered complex, Finland. *Can. Mineral.* **37**, 1507-1524.

_____, MARTIN, R.F., HALKOAHO, T.A.A. & CRIDDLE, A.J. (2002): Laflammeite, $Pd_3Pb_2S_2$, a new platinum-group mineral species from the Penikat layered complex, Finland. *Can. Mineral.* **40**, 671-678.

_____, _____, _____ & POIRIER, G. (2000): The mechanism of charge compensation in Cu–Fe–PGE thiospinels from the Penikat layered intrusion, Finland. *Am. Mineral.* **85**, 694-697.

_____, _____, MEN'SHIKOV, Y.P., SAVCHENKO, Y.E., THIBAULT, Y. & LAAJOKI, K.V.O. (2000): Edgarite, $FeNb_3S_6$, first natural niobium-rich sulfide from the Khibina alkaline complex, Russian Far North: evidence for chalcophile behavior of Nb in a fenite. *Contrib. Mineral. Petrol.* **138**, 229-236.

_____, THIBAULT, Y., LAAJOKI, K.V.O, MELEZHIK, V.A. & NILSSON, L.P. (1999b): Zoning and substitutions in Co–Ni–(Fe)–PGE sulfarsenides from the Mount General'skaya layered intrusion, Arctic Russia. *Can. Mineral.* **37**, 127-142.

BEGIZOV, V.D., ZAV'YALOV, E.N. & KHVOSTOVA, V.P. (1976): The minerals of the laurite–erlichmanite and hollingworthite–irarsite series from Urals placers. *Zap. Vses. Mineral. Obshchest.* **105**, 213-218 (in Russ.).

BERLINCOURT, L.E., HUMMEL, H.H., & SKINNER, B.J. (1981): Phases and phase relations of the platinum-group elements. *In* Platinum-Group Elements: Mineralogy, Geology, Recovery. (L.J. Cabri, ed.). *Can. Inst. Mining Metall., Spec. Vol.* **23**, 19-45.

BOWLES, J.F.W., ATKIN, D., LAMBERT, J.L.M., DEANS, T. & PHILLIPS, R. (1983): The chemistry, reflectance, and cell size of the erlichmanite (OsS_2) – laurite (RuS_2) series. *Mineral. Mag.* **47**, 465-471.

BREC, R., PROUZET, E. & OUVRARD, G. (1989): Redox processes in Li_xFeS_2 / lithium electrochemical system studied through crystal, Mössbauer, and EXAFS analyses. *J. Power Sources* **26**(3–4), 325-332.

BRENAN, J. M. & ANDREWS, D. (2001): High-temperature stability of laurite and Ru–Os–Ir alloy and their role in PGE fractionation in mafic magmas. *Can. Mineral.* **39**, 341-360.

CABRI, L.J., ed. (2002): The Geology, Geochemistry, Mineralogy, Mineral Beneficiation of the Platinum-Group Elements. *Can. Inst. Mining, Metall., Petroleum, Spec. Vol.* **54**.

_____, HARRIS, D.C. & WEISER, T.W. (1996): Mineralogy and distribution of platinum-group mineral (PGM) placer deposits of the world. *Explor. Mining Geol.* **5**, 73-167.

_____ & LAFLAMME, J.H.G. (1981): Analyses of minerals containing platinum-group elements. *In* Platinum-Group Elements: Mineralogy, Geology, Recovery. (L.J. Cabri, ed.). *Can. Inst. Mining Metall., Spec. Vol.* **23**, 151-173.

_____, LAFLAMME, J.H.G. & STEWART, J.M. (1977): Platinum-group minerals from Onverwacht. II. Platarsite, a new sulfarsenide of platinum. *Can. Mineral.* **15**, 385-388.

_____, _____, _____, TURNER, K. & SKINNER, B.J. (1978): On cooperite, braggite, and vysotskite. *Am. Mineral.* **63**, 832-839.

COLELL, H., ALONSO-VANTE, N., FIECHTER, S., SCHIECK, R., DIESNER, K., HENRION, W. & TRIBUTSCH, H. (1994): Crystal growth and properties of novel ternary transition metal chalcogenide compounds [$Ir_xRu_{1-x}S_2$ ($0.005 < x < 0.5$)]. *Mat. Res. Bull.* **29**, 1065-1072.

CRAIG, J.R. & SCOTT, S.D. (1974): Sulfide phase equilibria. *In* Sulfide Mineralogy (P.H. Ribbe, ed.). *Rev. Mineral.* **1**, CS1-110.

DE LOS REYES, J.A., VRINAT, M., GEANTET, C., BREYSSE, M. & GRIMBLOT, J. (1993): Supported ternary sulfide phases: characterization and catalytic properties of alumina-supported $Ni_xRu_{1-x}S_2$. *J. Catalysis* **142**, 455-464.

HALKOAHO, T.A.A, ALAPIETI, T.T. & LAHTINEN, J.J. (1990): The Sompujärvi PGE Reef in the Penikat layered intrusion, northern Finland. *Mineral. Petrol.* **42**, 39-55.

HOLZWARTH, N.A.W., HARRIS, S. & LIANG, K.S. (1985): Electronic structure of RuS_2. *Phys. Rev. B: Condens. Matter and Materials Phys.* **32**, 3745-3752.

HULLIGER, F. (1964): Crystal structure and electrical properties of some cobalt group chalcogenides. *Nature* **204**, 644-646.

HWANG SONG-TZER, LEE MING-CHIH, TSAY MING-YIH & HUANG YING-SHENG (1994): Raman scattering of $Fe_xRu_{1-x}S_2$ mixed crystals. *Japan. J. Appl. Phys., Part 1,* **33**, 6203-6206.

JEN YING-CHEN & TENG YU-JEN (1973): Isomorphous system RuS_2–OsS_2–IrS_2 and the mineral system PdS–PtS. *Geochimica* **4**, 254-263 (in Chinese).

JOBIC, S., BREC, R., PASTUREL, A., KOO, H.-J. & WHANGBO, M.-H. (2001): Theoretical study of possible iridium ditelluride phases attainable under high pressure. *J. Solid State Chem.* **162**, 63-68.

_____, DENIARD, P., BREC, R., ROUXEL, J., DREW, M.G.B. & DAVID, W.I.F. (1990): Properties of the transition metal dichalcogenides: the case of IrS_2 and $IrSe_2$. *J. Solid State Chem.* **89**, 315-327.

JUZA, R., HULSMANN, O., MEISEL, K. & BILTZ, W. (1935): The systematic doctrine of affinity. LXVI. The sulfides of rhodium. *Z. anorg. allgem. Chem.* **225**, 369-385.

KARUP-MØLLER, S. & MAKOVICKY, E. (2002): The system Fe–Os–S at 1180°, 1100° and 900°C. *Can. Mineral*. **40**, 499-507.

KJEKSHUS, A., RAKKE, T. & ANDRESEN, A.F. (1979): Pyrite-like phases in the rhodium–selenium system. *Acta Chem. Scand., Series A: Phys. and Inorg. Chem.* **A33**, 719-725.

LUTZ, H.D., MÜLLER, B., SCHMIDT, T. & STINGL, T. (1990): Structure refinement of pyrite-type RuS_2 and $RuSe_2$. *Acta Crystallogr., C: Crystal Structure Commun.* **C46**, 2003-2005.

MAKOVICKY, E., MAKOVICKY, M. & ROSE-HANSEN, J. (2002): The system Fe–Rh–S at 900° and 500°C. *Can. Mineral.* **40**, 519-526.

MUNSON, R.A. (1968): The synthesis of iridium disulfide and nickel diarsenide having the pyrite structure. *Inorg. Chem.* **7**, 389-390.

OHNENSTETTER, D., WATKINSON, D.H. & DAHL, R. (1991): Zoned hollingworthite from the Two Duck Lake intrusion, Coldwell complex, Ontario. *Am. Mineral*. **76**, 1694-1700.

SCHULER, M., DAHLEM, J. & SIEBERT, D. (1995): EPR investigation of synthetic, doped FeS_2 and RuS_2 single crystals. *Z. Naturforsch., A: Phys. Sciences* **50**, 1159-1164.

_____ & SIEBERT, D. (1995): EPR of Cr^{3+} and Fe^{3+} in RuS_2. *Phys. Status Solidi B: Basic Res.* **188**(2), K25-K28.

_____, _____ & EBLING, D.G. (1997): EPR of $^{57}Fe^{3+}$ and conductivity in RuS_2. *Appl. Phys. A: Mater. Science & Processing* **A64**, 203-206.

STINGL, T., MÜLLER, B. & LUTZ, H.D. (1992): Crystal structure refinement of OsS_2. *Z. Kristallogr.* **202**, 161-162.

TARKIAN, M., EVSTIGNEEVA, T.L. & GORSHKOV, A. (1996): Synthesis of Pt- and Pd-sulphides in low temperature (85°C) solutions buffered by clay minerals and graphite: preliminary results. *Mineral. Petrol.* **58**, 71-78.

TSAY MING-YIH, CHEN SHIMN-HORNG, CHEN CHIA-SHIN & HUANG YING-SHENG (1994): Preparation and characterization of iron-doped RuS_2 single crystals. *J. Crystal Growth* **144**, 91-96.

VERRYN, S.M.C. & MERKLE, R.K.W (2002): The system PtS–PdS–NiS between 1200° and 700°C. *Can. Mineral.* **40**, 571-584.

WEISER, T.W. & BACHMANN, H.-G. (1999): Platinum-group minerals from the Aikora river area, Papua New Guinea. *Can. Mineral.* **37**, 1131-1145.

WÖHLER, L., EWALD, K. & KRALL, H. (1933): The sulfides, selenides and tellurides of the six platinum metals. *G. Ber.* **66B**, 1638-1652.

WOOD, B.J. & STRENS, R.G. (1979): Diffuse reflectance spectra and optical properties of some sulphides and related minerals. *Mineral. Mag*. **43**, 509-518.

ZVIADADZE, G.N., GULYANITSKAYA, Z.F., BLAGOVESHCHENSKAYA, N.V., PAVLYUCHENKO, N.M., BLOKHINA, L.I. & RYABKO, A.G. (1981): Interaction of platinum with copper sulfides and ruthenium with nickel sulfides. *Izv. Akad. Nauk SSSR, Metally* **2**, 68-74 (in Russ.).

Received February 15, 2003, revised manuscript accepted March 31, 2004.